# OPTIMIZING STRUCTURE-PROPERTY RELATIONSHIPS IN DUCTILE IRON

**Dr. John M. Tartaglia, Richard B. Gundlach, George M. Goodrich**
Element Materials Technology, Wixom, MI, USA



## Abstract

*The purpose of this research was to identify ways to achieve a higher combination of strength and ductility, by characterizing the relationships between the graphite and metal matrix, alloy content, and tensile properties in ductile iron. The characterization utilized standard physical metallurgical tools including tensile properties, optical microscopy and automated image analysis to measure ferrite content, grain size, nodule count, nodule size and nodularity. In addition to applying standard statistical parameters such as mean and standard deviation, the study employed Pearson correlation coefficient analysis, transmission electron microscopy, and X-ray diffraction.*

*The overall objectives of the research were to:*

- *Identify chemical and matrix characteristics that might be used to optimize the relationship between graphite morphology, matrix, and mechanical properties.*
- *Optimize the control needed to produce the desired graphite and metal matrix relationships in a given section size to produce the desired mechanical properties.*
- *Improve the control and reduce the variation between mechanical properties measured in thin and heavy sections.*

*The principal investigators initially analyzed representative samples of grades 80-55-06 and 65-45-12 ductile iron; the compositions and tensile properties were measured and supplied by ten commercial foundries. From the original ten foundries, the investigators received additional samples of the two grades from four foundries and from an additional source. A total of 53 samples were subjected to hardness and mechanical testing. A total of 26 samples were subjected to further testing for composition, microstructure, and strain hardening behavior.*

*The results of the testing showed that the mechanical properties varied as expected with ferrite content. The strength increased as ferrite content decreased and ductility increased as ferrite content increased, and ferrite grains almost always touched graphite nodules. Manual and automated image analysis measurements of ferrite content showed excellent agreement. In addition, final work on selected samples from this study showed that the substructure of ferrite grains, as determined with X-ray diffraction or transmission electron microscopy, does not appear to influence ductile iron mechanical properties.*

*This study also determined that the combination of high strength (>80 ksi ultimate and >55 ksi yield) and high elongation (>12%) occurred when ferrite content was between 35 and 60%, and the ferrite colonies were discontinuous. Furthermore, the study also correlated the mechanical properties and microstructures to copper, manganese, silicon, and copper + manganese contents.*

*Subsequently, the authors investigated the desired alloy content relationship for developing these high strength-high elongation properties. An additional key objective was to investigate post solidification heat treatments to further optimize these composition-structure-property relationships.*

*To characterize the relationships between the graphite-metal matrix, alloy content, and tensile properties in ductile iron, the study utilized statistical tools to compute mean and standard deviation, Pearson correlation coefficient analysis, Student t-testing, and design of experiments (DOE) methodology.*

*The investigators conducted a DOE methodology where the following five key variables were investigated:*

- *Section size (1 inch versus 3 inch)*
- *Inoculation (ladle versus ladle plus in-stream)*
- *Silicon content (nominally 2.2 versus 2.7 wt-%)*
- *Manganese contents (0.2 versus 0.45 wt-%)*
- *Copper content (0.3 versus 0.6 wt-%)*

*All mechanical properties, including both strength and ductility, were lower in the 3 in. section size versus the 1 in. section size. Various statistical testing and DOE analysis showed that increasing Cu and/or Mn increased strength and hardness while decreasing ductility and toughness (UT) in both the 1 in. and 3 in. section sizes. In contrast, increasing Si decreased strength and increased ductility. However, varying Mn or Si was less effective than Cu in affecting the properties in the 1 in. section size. The authors recognize that all of these observations are consistent with the inherent knowledge that has developed during the lifetime of ductile iron. However, in this study the authors were able to begin the process of confirming and quantifying the relationships in a well-controlled dataset.*

*Based on the results of this study, the principal investigators chose to validate the DOE by casting additional 1 in.Y-blocks of one of the DOE heats, which contained 2.6%Si, 0.3%Mn and 0.6%Cu. The results were almost precisely duplicated with equivalent compositions, microstructures, strengths and ductilities.*

*The Principal Investigators also investigated post solidification heat treatments to refine grain size and further optimize these composition-structure-property relationships. Heat treatment trials were conducted by intercritically austenitizing and subjecting the samples to various cooling rates such as still air cool, forced air cool, and oil quenching, with the latter followed by tempering.*

*The most promising results were obtained with a starting microstructure of 50% ferrite and 50% pearlite. After heat treatment, the measured mechanical properties far exceeded some of the study goals of >55 ksi YS, >80 ksi ultimate tensile strength (UTS) and >12 % elongation. Even though 12% minimum elongation was not achieved through heat treatment, the quench and temper heat treatments produced much higher strength and equivalent ductility than many of the standard as-cast grades with equivalent ductility. Mechanical properties obtained after intercritical austenitizing followed by either air cooling or quench and temper heat treatment were as follows: 65 to 85 ksi yield strength (YS), 110 to 130 ksi UTS, and 8 to 9% elongation.*

***Keywords:*** *ductile iron, ferrite, pearlite, heat treatment, microstructure, strength, ductility*

## Introduction and Study Motivation

Researchers have devoted a significant amount of work to understand the relationship between solidification cooling rate and mechanical properties of ductile iron.[1-3] Significant work has also been conducted to relate some aspects of graphite morphology and mechanical properties.[4] The factors that remain elusive are processing variables that influence mechanical property variations that occur in the matrix when the graphite morphology seemingly remains unchanged.

This publication summarizes the results of a multiphase study to evaluate the ductile iron matrix contribution to mechanical properties. Only key results are included; for full details the reader should consult the project reports.[5-7]

ASTM A536 gives examples of the yield strength, tensile strength and elongation relationships expected in ductile cast iron. Table 1 below provides the information.

Frequently, both castings and separately cast test bars will exhibit mechanical properties that are significantly better than the required minimum values shown in Table 1. One example is the information generated from testing a ferritic ductile iron casting expected to have mechanical properties that would be consistent with Grade 65-45-12 in Table 1.

The properties measured by the authors, shown in Table 2,[8,9] reveal that Grade 80-55-06 properties were achieved, while still achieving the high elongation of Grade 65-45-12. The etched microstructure for this material is shown in Figure 1.[8,9]

This study was undertaken to build on the commercial observation of the aforementioned unconventional properties, some initial research, and to study the relationship between the structure and properties of ductile iron. The study searched for casting conditions that produced the unconventional properties with the strength of a pearlitic grade and the elongation of a ferritic grade, while using example materials from industry.

The study authors wanted to produce the following unique combination of strength and ductility properties *consistently*:

1. Yield strength greater than 55 ksi
2. Elongation greater than 12%
3. SAE J434 Grade D5506 (03)
4. ASTM A536 Grade 80-55-06

The study authors intended to develop an understanding of the relationship between alloying elements and properties in ductile iron that is not yet routinely available to ductile iron producers. This paper will review a Phase 1 study that included a commercial foundry survey, statistical analysis, and fracture path considerations. Then the paper summarizes how the authors planned for research casting, based on the Phase 1 results; the paper gives the research casting details, the sampling and DOE methodologies, and the effects of heat treatment.

***Table 1. ASTM A536-84(2009) Tensile Requirements, Minimum Values***

| Property | | Grade 60-40-18 | Grade 65-45-12 | Grade 80-55-06 | Grade 100-70-03 | Grade 120-90-02 |
|---|---|---|---|---|---|---|
| Tensile strength | psi | 60,000 | 65,000 | 80,000 | 100,000 | 120,000 |
| | MPa | 414 | 448 | 552 | 689 | 827 |
| Yield strength | psi | 40,000 | 45,000 | 55,000 | 70,000 | 90,000 |
| | MPa | 276 | 310 | 379 | 483 | 621 |
| Elongation in 2 in. or 50 mm | % | 18 | 12 | 6.0 | 3.0 | 2.0 |

## Literature Review

To the knowledge of the authors, no comprehensive research work has been conducted to determine what is required to consistently achieve 80-55-06 properties with a high amount of ferrite. The extraordinary properties shown in Table 2 were a prime motivation for extensively surveying the literature.

A global review of the cast iron literature from 1900 and ductile iron literature from 1948 to the present was conducted. The focus was on discerning published mechanisms related to grain size and impurity content that also produced enhanced strength and ductility. Of the 38 papers that fit the search criteria, nine were read in detail and common aspects identified. The Hall-Petch relationship[10-13] was confirmed in ferritic and austempered ductile iron. In both microstructures, examples were found where strength and ductility increased with smaller grain size. In addition, higher purity alloys and anisotropic dendritic structures were shown to enhance both strength and ductility.

The literature review showed that it was difficult to compare the results in the various papers because the alloys, processes, and metrics differed. Table 3 contains a comparison of the strengths and ductilities reported in the seven articles with the minimum values of two ASTM A536 grades. Interested individuals are referred to Reference 5 for more details about the literature review.

## The Commercial Foundry Data Survey

### Motivation

The objective of the first phase of this study was to survey the properties in commercial castings from several foundries. A key thrust was to investigate the chemistry and microstructural parameters that produced combinations of high strength and elongation.

### Sample Procurement

To obtain the information required for this investigation, the researchers estimated that a minimum of 50 ductile iron samples would be required. It was desired to have some of these samples reflect production castings with moderately high strength (>55 ksi yield strength) and high elongation (>12%) to compare with more traditional properties for the 65-45-12 and 80-55-06 grades.

Initially, samples were collected from ten foundries. Among those, the products from four foundries were selected for further study. The criteria used to select the four foundries related to the ability of the foundry to be consistent, their ability to produce the desired property range, and the evidence they provided regarding their quality control capabilities. Several foundries that submitted sample data fit these criteria and the decision was difficult. However, in the end, the selected four foundries provided 53 samples that served as the basis for this research. The principal investigators labeled these four foundries E, G, H, and J.

The submitted 53 samples were obtained from 1-in. keel blocks, 3-in. y-blocks, and sections from actual castings. Three additional casting samples were included by the authors. These additional samples were from a foundry customer that had indicated the material had performed exceptionally well in their application and that the material had the type of properties they were seeking for their ductile iron application. Interested parties can refer to Reference 5 for a comprehensive comparison of the processing parameters and an assessment of properties.

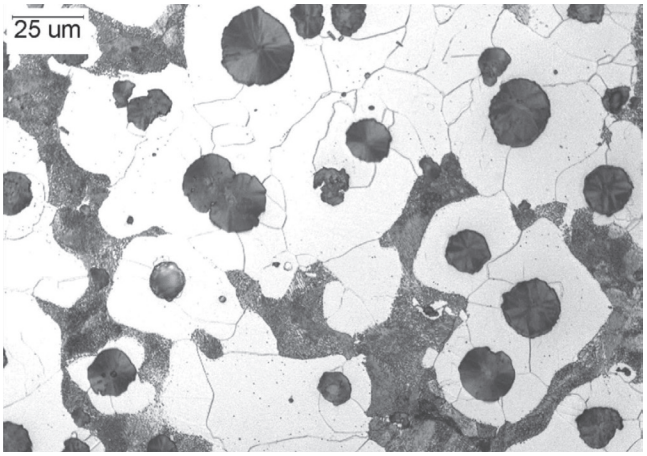


***Figure 1. Etched microstructure for the iron with the properties in Table 2.***

***Table 2. Mechanical Properties and Microstructure for a Commercial Casting***

| Ultimate Tensile Strength | | Yield Strength, 0.2% Offset | | % Elongation |
|---|---|---|---|---|
| MPa | ksi | MPa | ksi | % |
| 572 | 83.2 | 383 | 55.5 | 14.8 |
| % Pearlite | | % Ferrite | | % Nodularity |
| 32 | | 68 | | 95 |

***Table 3. Comparison of Elongation Values in the Literature versus Minimum 12% Requirement for Two ASTM A536 Ductile Iron Grades***

| Ref. # | UTS (MPa) | YS (MPa) | El (%) | Multiplier times ASTM minimum ductility | Comments on experimental value |
|---|---|---|---|---|---|
| *Grade 65-45-12 (448-310-12); minimum ductility = 12%* | | | | | |
| 14 | 415 | | 27 | 2.3 | d = 22 µm and λ=119 µm |
| 15 | 462 | | 12 | 1 | Perpendicular to dendrites |
| 16 | 448 | | 20 | 1.7 | C & Si levels and inoculation |
| *Grade 80-55-06 (552-379-06); minimum ductility = 6%* | | | | | |
| 15 | 565 | | 16 | 2.7 | Parallel to dendrites |
| 17 | 592 | | 11.4 | 1.9 | Unknown process/composition |
| 18 | 539 | 424 | 14.4 | 2.4 | Vanadium and grain size |
| 19 | 806 | 458 | 6.7 | 1.1 at 20 to 50% higher strength | As-cast condition with Sn added |
| 19 | 986 | 569 | 6.3 | 1.1 at 50 to 80% higher strength | Normalized condition with Sn added |

## Mechanical Testing

The investigators tested a total of 56 samples to determine tensile properties in accordance with ASTM E8 and Brinell hardness in accordance with ASTM E10. Brinell hardness was measured on 56 samples using 3,000 kg load and a 10mm diameter tungsten carbide ball. All tensile samples utilized a standard 0.505 in. diameter by 2 in. gauge length tensile bar, except for those obtained from the actual castings. Due to their small size, the castings were mostly tested using 0.35 in. gauge diameter and 1.4 in. gauge length specimens; a couple of casting samples were tested with 0.25 in. gauge diameter and 1 in. gauge length specimens.

Table 4 shows the descriptive statistics for all the mechanical testing conducted on the 56 commercial foundry samples. Reference 5 also contains a compilation of all the test data from these 56 samples.

After considering the mechanical property results from all 56 samples, 26 samples were selected for both qualitative and quantitative metallographic analysis as well as determination of monotonic strength coefficient and strain hardening exponent in accordance with ASTM E646. Table 5 shows the results for this parameter testing, as well as some less traditional variables that were calculated.

Perhaps terminology definitions[10] are needed for some of the more nontraditional variables, especially those that were calculated in Table 5. UTS is the ultimate tensile strength measured on the engineering stress-strain curve.

***Table 4. Descriptive Statistics for Measured Mechanical Properties on 53 Samples***

| Statistic | *Brinell Hardness* | *UTS (ksi)* | *YS (ksi)* | *% Elong.* | *%El (at Fracture)* | *%RA* | *Uniform Elongation (%)* |
|---|---|---|---|---|---|---|---|
| | | | | | | | |
| **Mean** | 200 | 87.2 | 53.4 | 14.3 | 14.3 | 13.4 | 12.0 |
| **Standard Error** | 3.3 | 1.83 | 0.88 | 0.75 | 0.72 | 0.88 | 0.43 |
| **Median** | 201 | 89.6 | 53.8 | 13.2 | 13.2 | 11.4 | 11.688 |
| **Mode** | 182 | #N/A | #N/A | #N/A | #N/A | 11.24 | #N/A |
| **Standard Deviation** | 24.2 | 13.31 | 6.40 | 5.43 | 5.26 | 6.37 | 3.10 |
| **Sample Variance** | 584.5 | 177.2 | 41.0 | 29.5 | 27.7 | 40.6 | 9.6 |
| **Kurtosis** | -0.79 | -0.96 | -0.37 | 0.30 | 0.23 | 0.32 | 0.81 |
| **Skewness** | 0.11 | -0.09 | 0.33 | 0.51 | 0.47 | 0.93 | -0.59 |
| **Range** | 98 | 49.28 | 26.7 | 22.308 | 21.055 | 24.719 | 12.886 |
| **Minimum** | 158 | 64.15 | 43.32 | 3.863 | 4.318 | 3.082 | 4.334 |
| **Maximum** | 256 | 113.43 | 70.02 | 26.2 | 25.373 | 27.801 | 17.22 |
| **Sum** | 10579 | 4623.7 | 2831.5 | 757.0 | 757.4 | 708.4 | 635.0 |
| **Count** | 53 | 53 | 53 | 53 | 53 | 53 | 53 |
| **Confidence Level(95.0%)** | 6.6639 | 3.6695 | 1.7643 | 1.4965 | 1.4509 | 1.7570 | 0.8538 |

***Table 5. Descriptive Statistics for Calculated Mechanical Properties (some on 53 and some on 24 samples)***

| Statistic | *(UTS-YS)/ YS (%)* | *Toughness, UT (ksi-in/in)* | *Strain Hardening Exponent, n* | *Section Modulus, In. (V/SA)* | *Statistic* |
|---|---|---|---|---|---|
| | | | | | |
| **Mean** | 0.63 | 9.6 | 0.213 | 0.37 | **Mean** |
| **Standard Error** | 0.010 | 0.33 | 0.0060 | 0.012 | **Standard Error** |
| **Median** | 0.632 | 9.9 | 0.207 | 0.40 | **Median** |
| **Mode** | #N/A | #N/A | 0.212 | 0.40 | **Mode** |
| **Standard Deviation** | 0.076 | 2.419 | 0.0294 | 0.088 | **Standard Deviation** |
| **Sample Variance** | 0.006 | 5.850 | 0.001 | 0.008 | **Sample Variance** |
| **Kurtosis** | -0.325 | 1.51 | 2.868 | 1.991 | **Kurtosis** |
| **Skewness** | -0.237 | -0.82 | 1.613 | -1.620 | **Skewness** |
| **Range** | 0.313 | 10.60 | 0.12 | 0.35 | **Range** |
| **Minimum** | 0.47 | 3.25 | 0.174 | 0.150 | **Minimum** |
| **Maximum** | 0.79 | 13.85 | 0.294 | 0.500 | **Maximum** |
| **Sum** | 33.22 | 510.48 | 5.119 | 19.838 | **Sum** |
| **Count** | 53 | 53 | 24 | 53 | **Count** |
| **Confidence Level(95.0%)** | 0.0209 | 0.6667 | 0.0124 | 0.0242 | **Confidence Level(95.0%)** |

YS is the yield strength measured at 0.2% offset strain on the engineering stress-strain curve. Percent elongation was measured on the test samples after failure. %El at fracture (by extensometer) was the total elongation determined with an extensometer during the tensile test, which is sometimes abbreviated $e_f$. Percent RA is the original area measured on the test specimen minus the fractured area of the test specimen, and the subtraction result is divided by the original area. Uniform elongation is the engineering strain to the point of the maximum load in an engineering stress-strain curve.

The difference between the ultimate tensile and yield strengths (UTS-YS) and

$$SH = 100 * (UTS - YS)/YS \quad \text{Eqn. 1}$$

are methods of characterizing the strengthening in the plastic strain range,[20] normalizing the data for comparison purposes. Toughness $U_T$ (ksi-in/in) is related to the area under the stress-strain curve, as approximated[10] for a ductile material by the following formula:

$$U_T = \tfrac{1}{2} * (YS+UTS) * e_f \quad \text{Eqn. 2}$$

The strain hardening exponent (n) is the slope of log true stress versus log true strain line in the plastic strain regime, and the monotonic strength coefficient (K) is the true stress at a true strain of unity.

One reason that the investigators determined the n-value was the initial hypothesis that decreasing slope of the stress-strain curve would allow ductile iron producers to achieve more elongation at a given strength value. Accordingly, this would maximize the likelihood of achieving the goal of this research, namely high strength ductile iron with high elongation.

## Metallography and Chemical Analysis

Transverse metallographic samples were obtained from the shoulders of all 26 tensile samples selected for more intensive metallographic analysis. In some cases, longitudinal samples were sectioned and these included the entire gauge section and fracture surface. All samples were mounted, polished, and etched in accordance with ASTM E3.

Ferrite content, nodule count and nodularity were determined by image analysis in accordance with ASTM A247 and E1245. Grain size was determined manually by the comparison method in accordance with ASTM E112. Chemical analysis was conducted on the samples in such a way that at least two samples per each grade and foundry were analyzed. The carbon and sulfur contents were determined combustometrically and glow discharge spectroscopy was used to determine all other elemental contents.

The compositions are shown in Table 6. The quantitative metallographic analysis results are presented in Tables 7 and 8 for the graphite and matrix characterization, respectively.

## Correlation Analysis

Microsoft Office Excel® was used to conduct Pearson Correlation Analyses. Correlation is a measure of the relation between two or more variables. References 5 and 7 contain the Pearson correlation matrix for all of the variables that were measured or calculated. The results were organized by groupings of measured mechanical test results, calculated mechanical properties, compositions and quantitative metallographic results.

Correlation is a measure of the relation between two or more variables. The measurement scales used should be at least interval scales, but other correlation coefficients are available to handle other types of data. Correlation coefficients can range from -1.00 to +1.00. The value of -1.00 represents a perfect negative correlation while a value of +1.00 represents a perfect positive correlation. A value of 0.00 represents a lack of correlation.

***Table 6. Compositions Representing 56 Selected Samples, Wt%***

| Overall Sample # | Foundry | Grade | Cast Section Size | C | S | P | Si | Mn | Cr | Ni | Mo | V | Al | Cu | Mg | Ti | Sb | Ce | Sn | Carbon Equivalent (CE) |
|---|---|---|---|---|---|---|---|---|---|---|---|---|---|---|---|---|---|---|---|---|
| 0A | AA | 80-55-06 | 1" Wall cylinder | 3.54 | 0.010 | 0.022 | 2.73 | 0.38 | 0.06 | 0.09 | 0.12 | 0.006 | 0.017 | 0.12 | 0.043 | 0.011 | <0.005 | 0.014 | <0.005 | 4.46 |
| 0B | AA | 80-55-06 | 1" Wall cylinder | 3.54 | 0.010 | 0.022 | 2.73 | 0.38 | 0.06 | 0.09 | 0.12 | 0.006 | 0.017 | 0.12 | 0.043 | 0.011 | <0.005 | 0.014 | <0.005 | 4.46 |
| 0C | AA | 80-55-06 | small piece | 3.48 | 0.008 | 0.022 | 2.77 | 0.44 | 0.09 | 0.04 | 0.15 | <0.005 | 0.020 | 0.27 | 0.052 | 0.014 | <0.005 | 0.013 | <0.005 | 4.41 |
| 1 | E | 65-45-12 | 1" keel blocks | 3.56 | 0.007 | 0.011 | 2.67 | 0.18 | 0.06 | 0.06 | <0.01 | 0.014 | 0.012 | 0.2 | 0.046 | 0.011 | <0.005 | 0.009 | <0.005 | 4.45 |
| 10 | E | 65-45-12 | 1" keel blocks | 3.56 | 0.008 | 0.012 | 2.67 | 0.18 | 0.06 | 0.06 | <0.01 | 0.016 | 0.012 | 0.20 | 0.045 | 0.011 | <0.005 | 0.009 | <0.005 | 4.45 |
| 11 | E | 80-55-06 | 1" keel blocks | 3.59 | 0.007 | 0.011 | 2.66 | 0.29 | 0.06 | 0.06 | <0.01 | 0.017 | 0.012 | 0.43 | 0.047 | 0.011 | <0.005 | 0.009 | <0.005 | 4.48 |
| 21 | E | 80-55-06 | 1" keel blocks | 3.57 | 0.007 | 0.011 | 2.66 | 0.29 | 0.06 | 0.06 | <0.01 | 0.016 | 0.013 | 0.42 | 0.05 | 0.011 | <0.005 | 0.011 | <0.005 | 4.46 |
| 22 | G | 80-55-06 | 3" Y-blocks | 3.51 | 0.007 | 0.014 | 2.28 | 0.44 | 0.06 | 0.21 | 0.27 | 0.016 | 0.015 | 0.57 | 0.037 | 0.020 | <0.020 | 0.004 | <0.005 | 4.27 |
| 23 | G | 80-55-06 | 3" Y-blocks | 3.48 | 0.006 | 0.017 | 2.25 | 0.35 | 0.07 | 0.21 | 0.23 | 0.011 | 0.016 | 0.58 | 0.040 | 0.020 | <0.020 | 0.006 | <0.005 | 4.24 |
| 25 | H | 65-45-12 | Casting | 3.44 | <0.005 | 0.018 | 2.51 | 0.34 | 0.06 | 0.02 | <0.01 | 0.007 | 0.008 | 0.46 | 0.033 | 0.013 | <0.005 | 0.012 | <0.005 | 4.28 |
| 26 | H | 65-45-12 | 0.6" Casting | 3.53 | <0.005 | 0.025 | 2.62 | 0.37 | 0.07 | 0.02 | <0.01 | 0.009 | 0.016 | 0.35 | 0.042 | 0.016 | <0.005 | 0.012 | <0.005 | 4.41 |
| 34 | J | 65-45-12 | 1" keel blocks | 3.63 | <0.005 | 0.023 | 2.47 | 0.31 | 0.08 | 0.05 | <0.01 | 0.016 | 0.013 | 0.30 | 0.037 | 0.013 | <0.005 | 0.005 | <0.005 | 4.46 |
| 43 | J | 65-45-12 | 1" keel blocks | 3.68 | <0.005 | 0.022 | 2.47 | 0.31 | 0.08 | 0.04 | <0.01 | 0.014 | 0.012 | 0.30 | 0.036 | 0.013 | <0.005 | 0.003 | <0.005 | 4.51 |
| 44 | J | 80-55-06 | 1" keel blocks | 3.66 | <0.005 | 0.024 | 2.49 | 0.33 | 0.09 | 0.04 | <0.01 | 0.019 | 0.016 | 0.48 | 0.034 | 0.012 | <0.005 | 0.004 | <0.005 | 4.50 |
| 53 | J | 80-55-06 | 1" keel blocks | 3.66 | <0.005 | 0.026 | 2.47 | 0.33 | 0.09 | 0.04 | <0.01 | 0.021 | 0.014 | 0.47 | 0.037 | 0.013 | <0.005 | 0.003 | <0.005 | 4.49 |

*Table 7. Quantitative Metallographic Results for Graphite on 26 Selected Samples*

| Overall Sample # | Foundry | Grade | Cast Section Size | Automated Image Analysis[b] | | | | | | | Manual Measurements | |
|---|---|---|---|---|---|---|---|---|---|---|---|---|
| | | | | Nodularity | Nodule Count | # of Class | | | | Maximum Nodule Size | Graphite Volume Fraction | Other observations |
| | | | | | | 7 | 6 | 5 | 4[a] | | | |
| | | | | (%) | ($mm^{-2}$) | (%) | | | | (µm) | (%) | |
| 0A | AA | 80-55-06 | 1" Wall | 95 | 146 | 28 | 51 | 21 | 0.12 | 89.8 | 11 | |
| 0B | | | 1" Wall | 93 | 70 | 17 | 35 | 47 | 1.13 | 100.8 | 9 | |
| 3 | E | 65-45-12 | 1" keel blocks | 94 | 160 | 25 | 57 | 18 | 0.07 | 87 | 11 | |
| 4 | | | | 93 | 185 | 33 | 55 | 12 | 0.03 | 84 | 10 | |
| 10 | | | | 93 | 169 | 28 | 56 | 16 | 0.03 | 86 | 11 | |
| 11 | | 80-55-06 | | 94 | 144 | 27 | 54 | 19 | 0 | 78 | 10 | Duplex nodules |
| 13 | | | | 97 | 184 | 29 | 59 | 12 | 0.03 | 89 | 10 | |
| 15 | | | | 96 | 160 | 26 | 57 | 16 | 0.11 | 99 | 10 | |
| 20 | | | | 95 | 198 | 34 | 56 | 10 | 0 | 77 | 10 | |
| 21 | | | | 96 | 182 | 28 | 57 | 14 | 0.03 | 82 | 11 | |
| 22 | G | 80-55-06 | 3" Y-blocks | 95 | 52 | 16 | 26 | 50 | 8.4 | 128 | 10 | Some Type IV graphite & low graphite count |
| 23 | | 80-55-06 | 3" Y-blocks | 83 | 82 | 21 | 46 | 31 | 2.92 | 129 | 9 | |
| 24 | H | 65-45-12 | 0.6" Casting | 95 | 294 | 65 | 30 | 5 | 0 | 60 | 9 | Duplex nodules |
| 25 | | | Casting | | | | | | | | | |
| 26 | | | 0.6" Casting | 97 | 410 | 72 | 27 | 2 | 0 | 57 | 10 | Duplex nodules |
| 27 | | | 0.75" Casting | | | | | | | | | |
| 28 | | | 0.9" Casting | 96 | 147 | 21 | 53 | 26 | 0.04 | 81 | 11 | Duplex nodules |
| 29 | | | 0.8" Casting | 97 | 408 | 65 | 32 | 3 | 0 | 64 | 12 | |
| 30 | | | Casting | 97 | 249 | 42 | 50 | 9 | 0 | 69 | 11 | Dirty |
| 31 | | | 0.9" Casting | | | | | | | | | |
| 32 | | | 0.5" Casting | 97 | 299 | 43 | 55 | 2 | 0 | 57 | 11 | Large pores |
| 33 | | | 0.5" Casting | 97 | 142 | 18 | 54 | 28 | 0 | 77 | 11 | Intercellular carbides |
| 34 | J | 65-45-12 | 1" keel blocks | 97 | 189 | 25 | 62 | 13 | 0 | 72 | 11 | |
| 37 | | | | 98 | 232 | 32 | 59 | 9 | 0 | 77 | 12 | |
| 38 | | | | 98 | 193 | 26 | 61 | 13 | 0 | 66 | 11 | |
| 40 | | | | 96 | 172 | 24 | 58 | 18 | 0 | 78 | 11 | |
| 51 | | 80-55-06 | | 98 | 201 | 28 | 60 | 12 | 0 | 78 | 11 | |
| 52 | | | | 98 | 214 | 32 | 58 | 10 | 0 | 69 | 11 | |
| 53 | | | | 98 | 190 | 27 | 60 | 13 | 0.03 | 83 | 11 | |
| a | No class 3 or larger nodules were detected | | | | | | | | | | | |
| b | All automated image analysis was conducted on 25 fields for a total analyzed area of 17.6 $mm^3$. | | | | | | | | | | | |

## Discussion of Commercial Foundry Data Survey

### Mechanical Testing and Microstructural Analysis

The authors compiled all of the data into a single Excel workbook and subjected the results to copious statistical evaluations. The initial step was to construct a correlation matrix. The variables used for the correlation matrix included all of the measured properties; the calculated properties for the 56 samples; the microstructures for the 26 samples; and the composition. The microstructure variables included all of the matrix features measured with image analysis, ferrite content, pearlite content, and carbide; the ferrite content determined manually; the ferrite grain size determined manually; and the graphite features measured with image analysis, including graphite nodule count, nodularity, and nodule size. Mechanical properties were correlated with Mn, Cu and Si contents. Strength and hardness were positively correlated (increased) with increasing Mn and Cu contents, whereas ductility was negatively correlated with those elements. Silicon had the opposite effects on mechanical properties. Strength and ductility values were negatively correlated, as would be expected.

Much of the information to be presented in this report involves use of automated image analysis (IA). In some cases, comparisons are made with manual measurements where IA was not used. Therefore, a comparison was made between visual estimation of ferrite content and IA analysis of ferrite content, which is the only parameter that was measured by both methods. The results are shown in Figure 2.

*Table 8. Quantitative Metallographic Results for Matrix on 26 Selected Samples*

| Overall Sample # | Foundry | Grade | Cast Section Size | Automated Image Analysis[c] | | Manual Measurements | | | | | | |
|---|---|---|---|---|---|---|---|---|---|---|---|---|
| | | | | Mean Ferrite Volume Fraction | Std Dev Ferrite Volume Fraction | Ferrite Grain Size | | Ferrite Volume Fraction | | Pearlite Volume Fraction | | Other observations |
| | | | | | | Near-Nodules | Matrix | Surface | Core | Surface | Core | |
| | | | | (%) | (%) | ASTM # | | (%) | (%) | (%) | (%) | |
| 0A | AA | 80-55-06 | 1" Wall | 35 | 2.4 | 10.6 | 9.6[b] | | | | | |
| 0B | | | 1" Wall | 19 | 1.9 | 9.6 | 8.1[b] | | | | | |
| 3 | E | 65-45-12 | 1" keel blocks | 86 | 1.5 | 7.5 | 5.5 | 93 | 97 | 7 | 3 | Trace nitrides |
| 4 | | | | 85 | 1.4 | 7.5 | 5.0 | 93-95 | | 5 to 7 | | Trace nitrides |
| 10 | | | | 92 | 1.4 | 8.0 | 6.0 | 97-100 | | 0-3 | | Trace nitrides, intercellular carbides |
| 11 | | 80-55-06 | | 32 | 2.2 | 5.5 | 5.0 | 20 | | 80 | | Duplex nodules, porosity |
| 13 | | | | 62 | 2.6 | 7.5 | 5.5 | 60 | 65 | 40 | 35 | Trace nitrides |
| 15 | | | | 39 | 2.0 | 7.0 | 6.0 | 35 | 40 | 65 | 60 | Trace nitrides, porosity |
| 20 | | | | 58 | 4.3 | 7.5 | 6.0 | 75 | | 25 | | |
| 21 | | | | 56 | 4.4 | 6.5 | 6.0 | 65 | | 35 | | |
| 22 | G | 80-55-06 | 3" Y-blocks | 0.21 | 0.12 | 8.5 | 8.5 | 5 | | 95 | | Trace nitrides, intercellular carbides, porosity |
| 23 | | 80-55-06 | 3" Y-blocks | 2 | 0.6 | 8.5 | 8.5 | 7 | | 93 | | Trace nitrides, intercellular carbides, microporosity at surface |
| 24 | H | 65-45-12 | 0.6" Casting | 22 | 1.3 | 7.0 | 6.5 | 15 | | 85 | | Dirty |
| 25 | | | Casting | | | | | | | | | |
| 26 | | | 0.6" Casting | 48 | 1.9 | 7.0 | 6.0 | 40 | | 60 | | |
| 27 | | | 0.75" Casting | | | | | | | | | |
| 28 | | | 0.9" Casting | 52 | 4.1 | 7.0 | 5.5 | 85 | 75 | 15 | 25 | Intercellular carbides, microporosity |
| 29 | | | 0.8" Casting | 65 | 2.6 | 8.0 | 6.0 | 60 | | 40 | | |
| 30 | | | Casting | 65 | 2.4 | 6.0 | 5.0 | 75 | | 25 | | Dirty |
| 31 | | | 0.9" Casting | | | | | | | | | |
| 32 | | | 0.5" Casting | 26 | 5.3 | 7.0 | 7.0 | 10 | 15 | 90 | 85 | Large pores |
| 33 | | | 0.5" Casting | 35 | 2.2 | 5.5 | 5.0 | 70 | 40 | 30 | 60 | Intercellular carbides |
| 34 | J | 65-45-12 | 1" keel blocks | 60 | 2.7 | 7.0 | 5.5 | 50 | | 50 | | |
| 37 | | | | 70 | 3.3 | 7.0 | 6.0 | 80-85 | | 15-20 | | Trace nitrides, secondary carbides |
| 38 | | | | 54 | 3.2 | 8.0 | 7.0 | 60-65 | | 35-40 | | |
| 40 | | | | 70 | 4.4 | 6.5 | 6.0 | 75-80 | | 20-25 | | Trace nitrides, minor porosity |
| 51 | | 80-55-06 | | 36 | 2.1 | 7.0 | 5.5 | 40 | 45 | 60 | 55 | Trace nitrides |
| 52 | | | | 38 | 3.0 | 7.0 | 6.0 | 40 | | 60 | | Trace nitrides |
| 53 | | | | 41 | 3.0 | 8.0 | 5.5 | 50 | 50 | | | |
| a | No class 3 or larger nodules were detected | | | | | | | | | | | |
| b | All grain sizes were estimated at 200X, except for these two acicular samples which were measured at 500X. Measured grain size number was converted to 100X per mathematical relationship in ASTM E112. | | | | | | | | | | | |
| c | All automated image analysis was conducted on 25 fields for a total analyzed area of 17.6 $mm^3$. | | | | | | | | | | | |

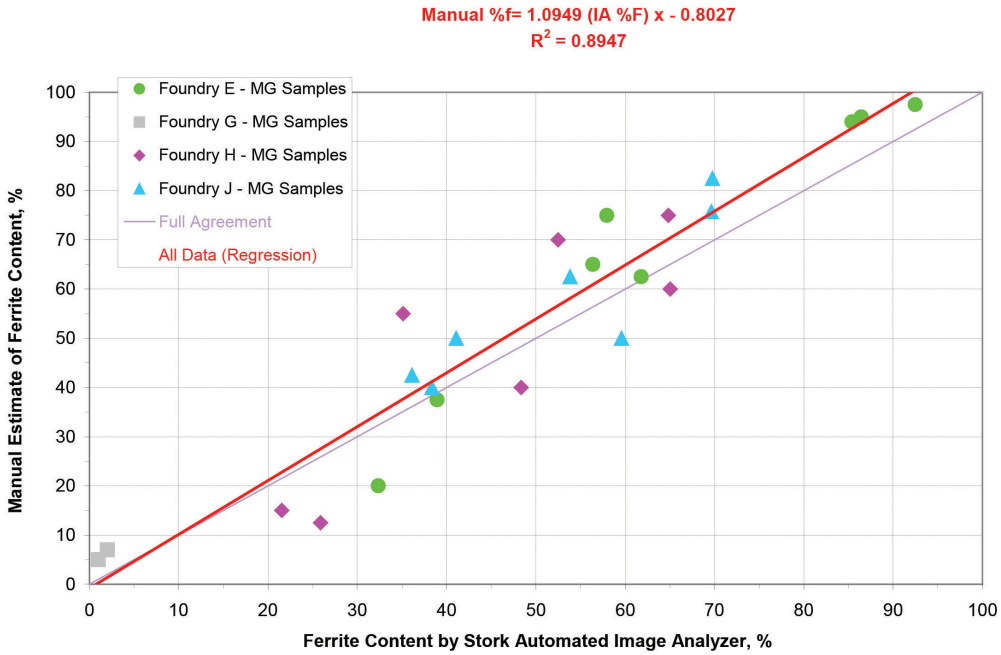


*Figure 2. Comparison of automated image analysis v. manual ferrite content determinations.*

The correlation was outstanding in that high linearity was observed, as represented by a coefficient of determination ($R^2$) of nearly 0.9, and a slope of 1.09, which was nearly unity.

All of the mechanical properties behaved in accordance with expectations based on ferrite content. Namely, as ferrite content increased, ductility increased, ultimate tensile strength decreased, and yield strength decreased. Figure 3 documents this relationship for tensile strength. (Note that this figure only has 24 samples because quantitative metallographic measurements for ferrite content were unavailable from 2 of the 26 samples summarized in Table 8.)

Previous investigators[1-3] have demonstrated that section size (cooling rate) had an influence over these properties as well. Although in the initial part of this current study, section size was not determined to be a factor, the reader should keep in mind that the evaluated samples did not allow the assessment of a section size effect. This aspect is important and should be a factor that is studied in the second phase of this project. Considering that the two Foundry G samples (the gray boxes on Figures 3 to 5) had the least amount of ferrite, they did not display the highest ultimate strength or yield strength.

Figures 4 to 6 show that reasonable correlations were obtained between strength, ductility and hardness, regardless of microstructure in the 53 samples from the foundries that formally participated in the study, i.e., the three samples from the commercial foundry that were labeled Foundry "AA" in Tables 6 to 8 were excluded from the figures.

Although the two Foundry G samples have, by far, the highest pearlite content of the 53 foundry samples, their 235-240 HB hardness values were not the highest, indicating that section size (cooling rate) has an influence. Because of the limited range of sections studied, the section size effect was not determined in this phase of the investigation.

Figures 6 and 7 show that elongation generally decreased with increasing hardness and strength, and there was significant data scatter at lower elongation values (below 12%). This scatter indicates that microstructure may play a greater role in determining elongation than in determining strength.

Figure 8 shows that the ferrite grain size was generally finer next to the graphite nodules versus those in "the matrix" interior for any given value of yield strength.

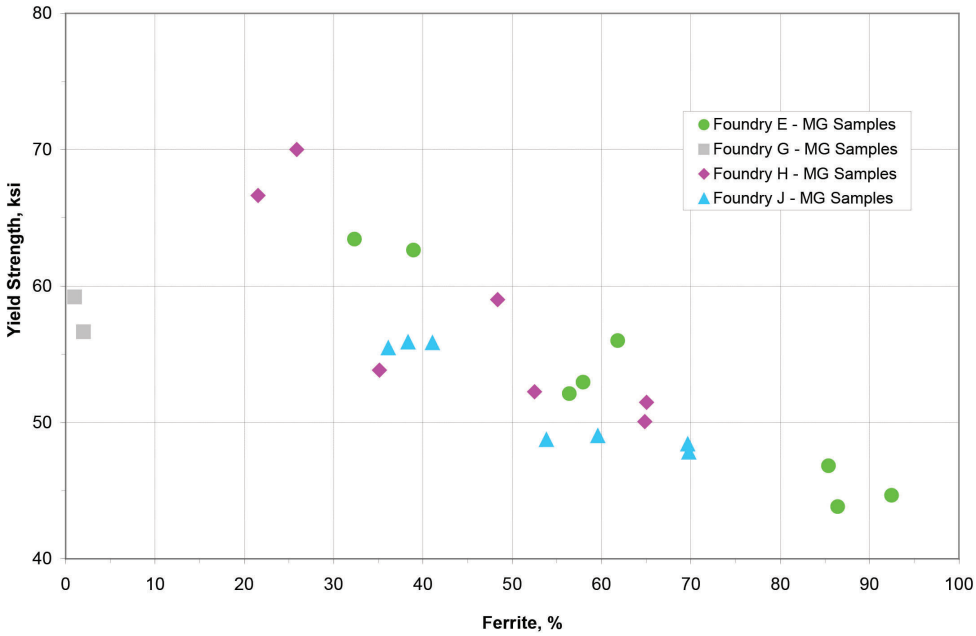


***Figure 3. Yield strength v. ferrite content for 24 selected samples.***

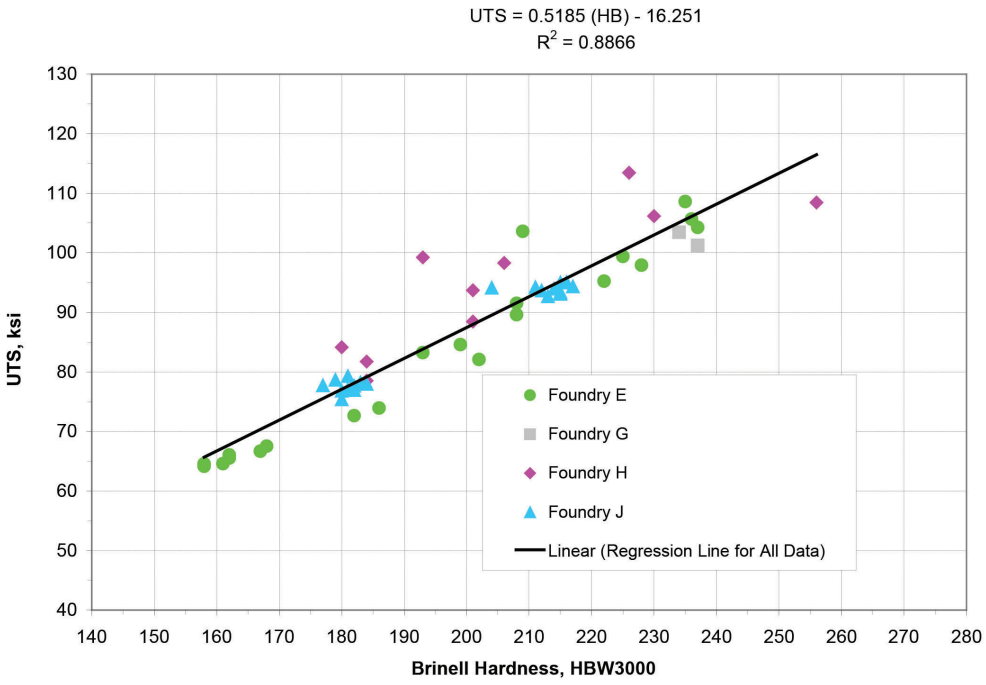


***Figure 4. Ultimate tensile strength v. Brinell hardness for the entire 53 foundry sample set.***

Figure 4 showed that strength varied with one microstructural parameter (ferrite content); a similar result was obtained for ductility.[5,7] Although the literature suggested that there might be a Hall-Petch ferrite grain size effect and the initial author study suggested it might be present, Figure 8 shows that yield strength did not vary with grain size for the commercial foundry sampling, and similarly insignificant variation was found when correlating UTS v. grain size as well as elongation v. grain size.

For all the standard tensile properties v. grain size, linear regression analysis produced low coefficients of determination (≈ 0.1) for all six correlations. (There were six correlations because investigators separately considered UTS, YS, and elongation versus grain size, which was measured both adjacent to nodules and in the matrix.) Furthermore, plotting the strength data in the standard $d^{-½}$ Hall-Petch format would lead to the same conclusion because the grain size varied so little in this study. It is possible that this limited ferrite grain size versus Hall-Petch variation is truly representative of ductile iron overall. One reason may be that factors such as the presence of graphite nodules may be of greater influence, or at least disguise a Hall-Petch grain size trend in ductile iron.

## Alloy Content Considerations

Additional evaluations were conducted with the data to determine the effects of composition. The relationship between certain elements and ferrite content was of specific interest, particularly since the ductile iron industry uses copper, manganese, and tin to control the pearlite content of the matrix. As shown in Table 6, none of the foundries in this investigation used tin.

As expected, based on over 60 years of experience with casting ductile iron, the correlation matrix (see Table 11) indicated that silicon has a positive correlation with ferrite content. Furthermore, in decreasing order, copper, manganese, titanium, molybdenum, and antimony are elements that exhibit a negative correlation with the occurrence of ferrite

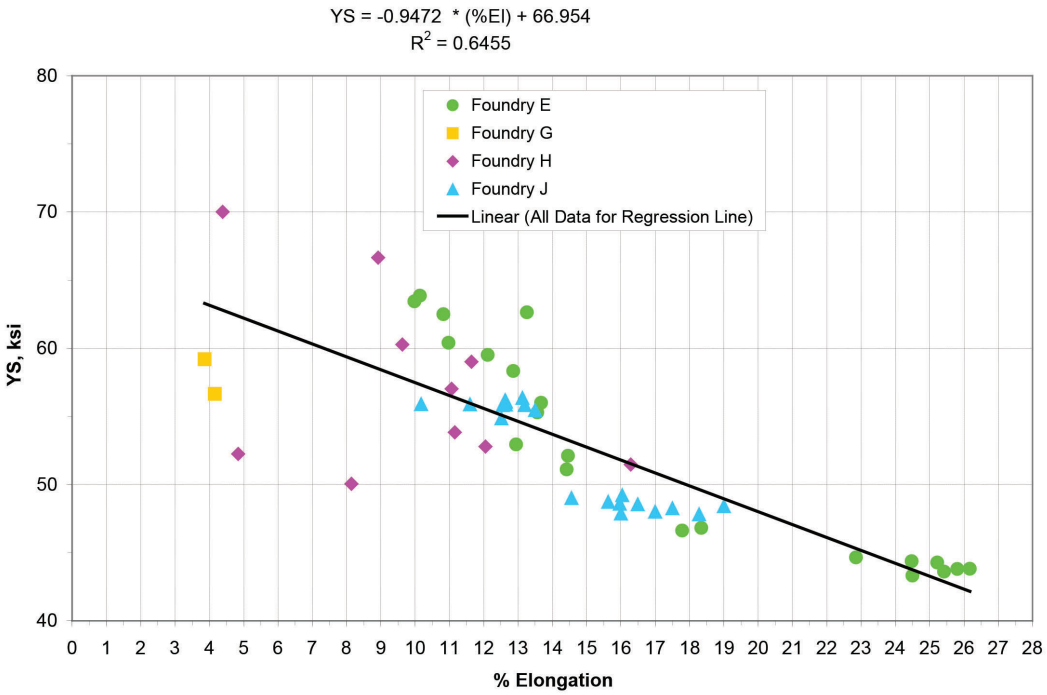


*Figure 5. Yield strength v. Brinell hardness for the entire 53 foundry sample set.*

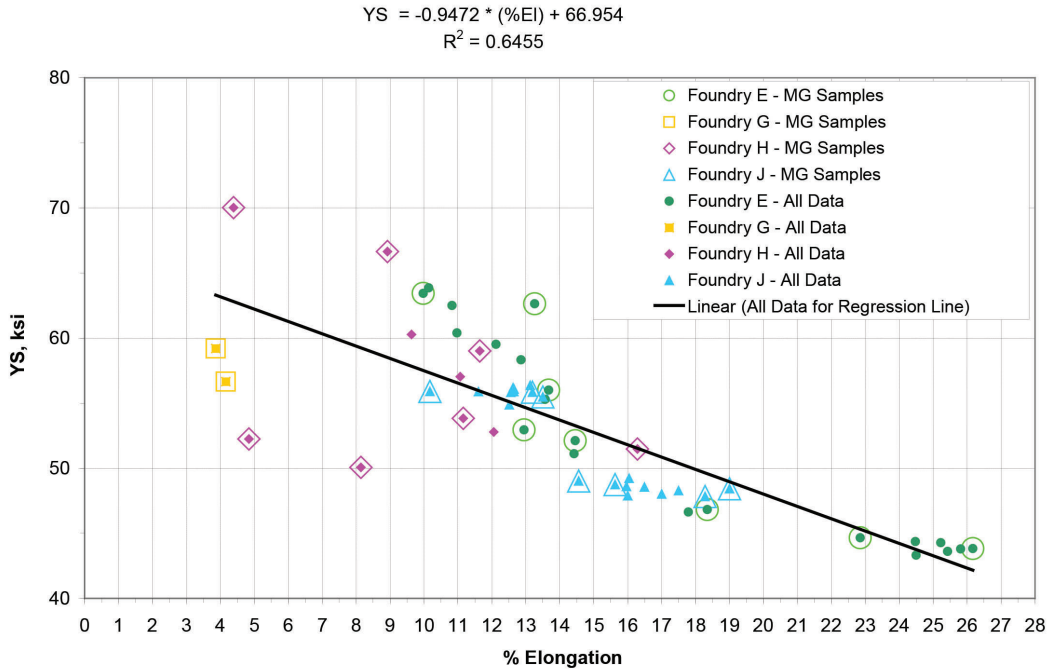


*Figure 6. Yield strength v. elongation for the entire 53 foundry sample set.*

content. The combined copper and manganese contents had the strongest negative correlation. However, Table 6 shows that there were only two molybdenum content and two antimony content levels.

The principal investigators of this study recognize that the correlations with the elements stated above are restricted to the ranges that were studied in this investigation and that the number of data points are inconsistent with the guidelines expected for acceptable statistical analysis. However, the foundry data survey phase of this investigation was intended to identify trends that could be more stringently pursued subsequently in the investigation. With this understanding, Figures 9 to 12 and the other results[5,7] show the relationships between mechanical properties and the contents of elements that exhibited high correlation coefficients with yield strength and elongation.

This analysis indicates that the combination of the desired yield strength (~55 ksi) and elongation (> 12%), one of the goals of this investigation, requires the following conditions:

- final silicon content of 2.48 to 2.68%;
- copper content of 0.40 to 0.48%;
- manganese content of 0.28 to 0.33%; and
- the copper + manganese contents of 0.7% to • 0.8%.

The plots also indicate that when lowering the copper to 0.3% (while maintaining Cu+Mn equal to 0.7 to 0.8%), the elongation increases above 15% but the yield strength falls to below 50 ksi.

Using three-dimensional plotting capability and viewing the relationships via the bubble presentation permits further assessment of strength and ductility data with respect to ferrite content. This three-variable correlation is shown in Figure 13.

Essentially, Figure 13 shows that the "ideal ferrite" content ranged from 40 to 60% for achieving the combination of ≥ 55 ksi yield strength and ≥ 10% elongation.

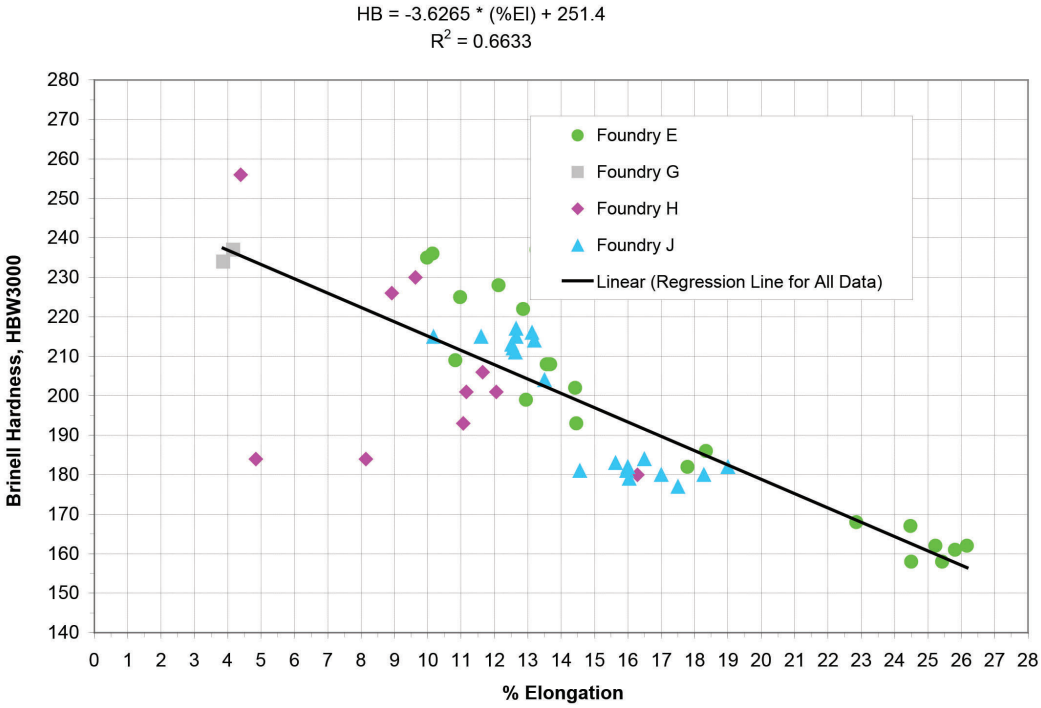


*Figure 7. Elongation v. Brinell hardness for the entire 53 foundry sample set.*

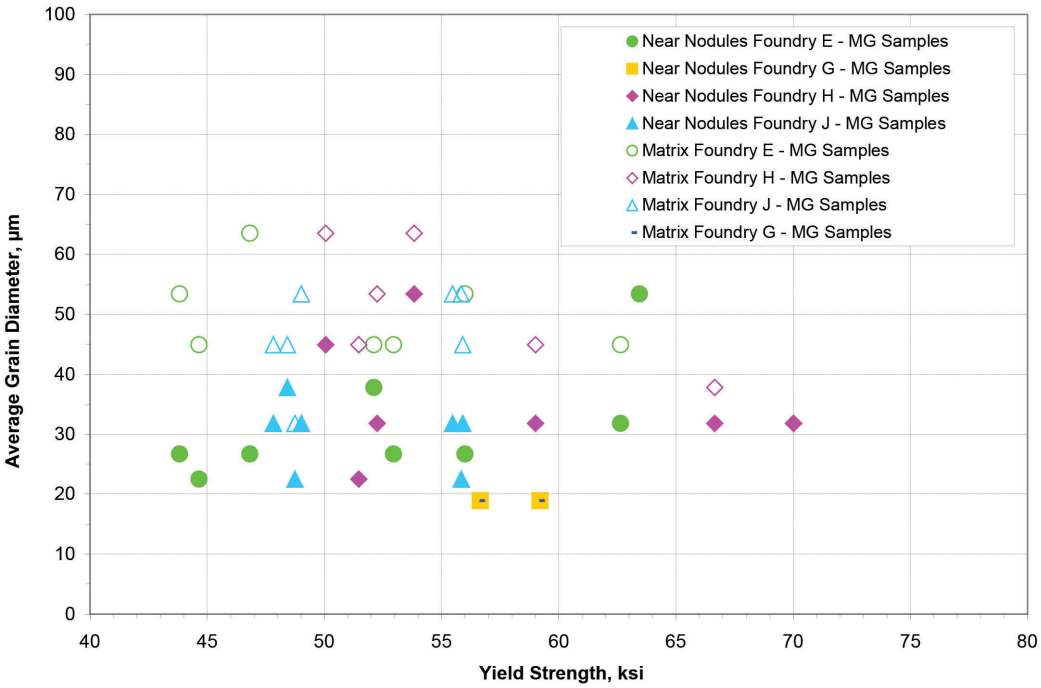


*Figure 8. Ferrite grain size v. yield strength for 24 selected samples.*

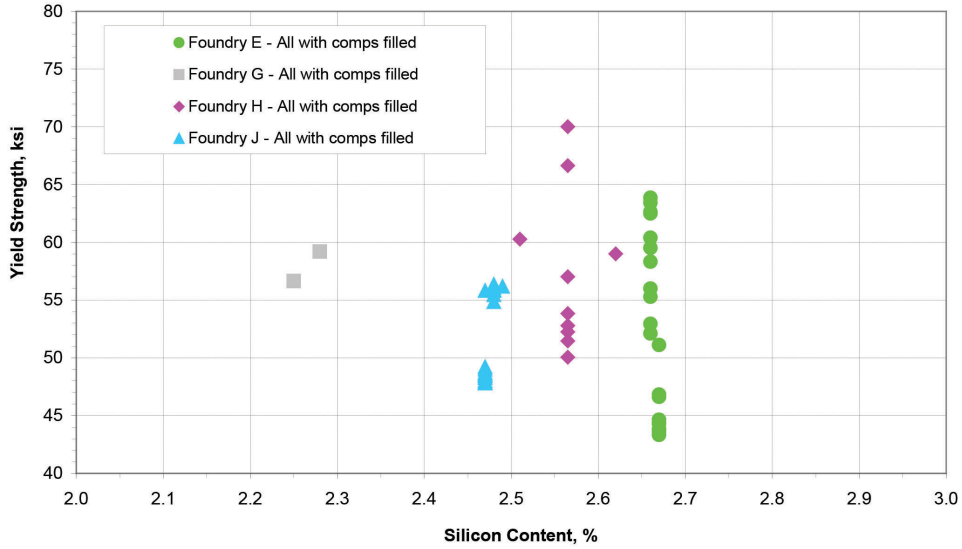


*Figure 9. Yield strength v. silicon content for the 53 samples.*

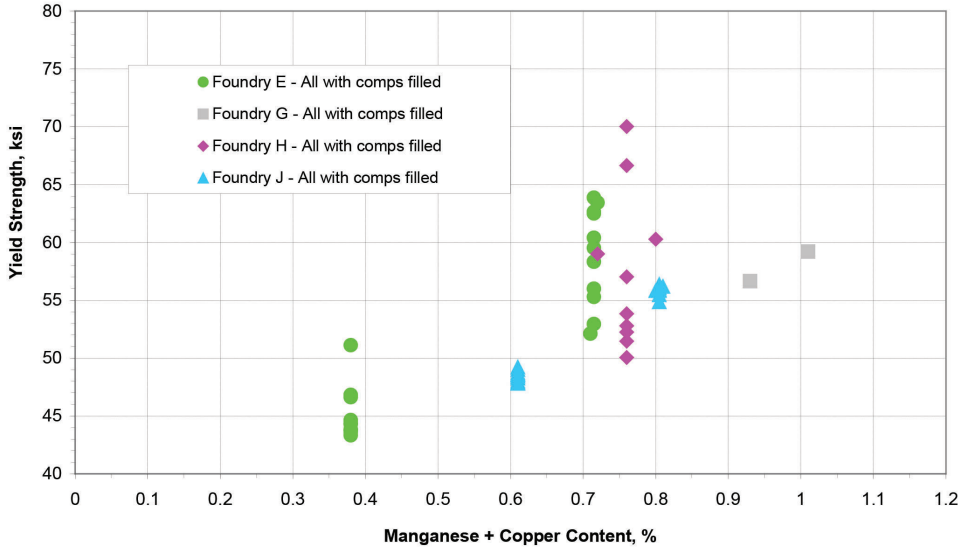


*Figure 10. Yield strength v. copper + manganese contents for the 53 samples.*

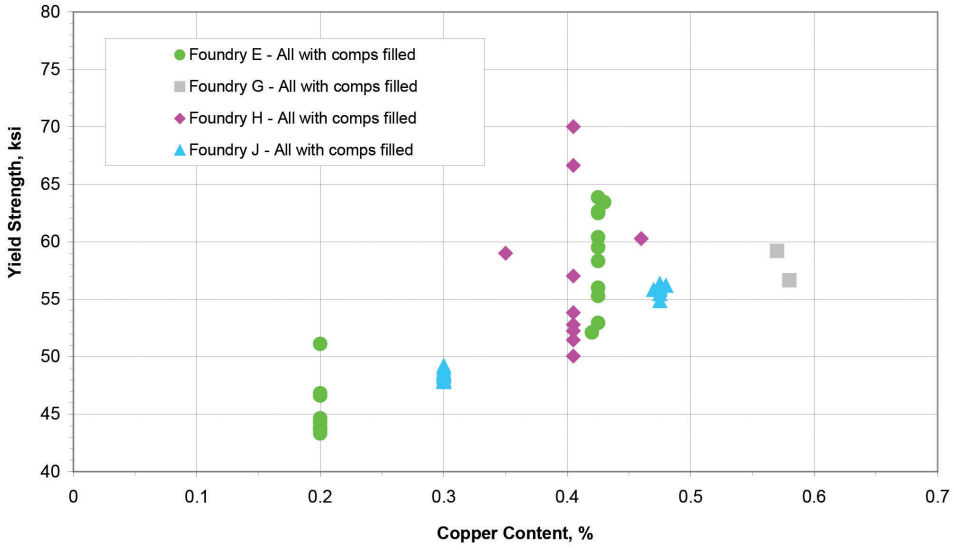


*Figure 11. Yield Strength v. Copper content for the 53 samples.*

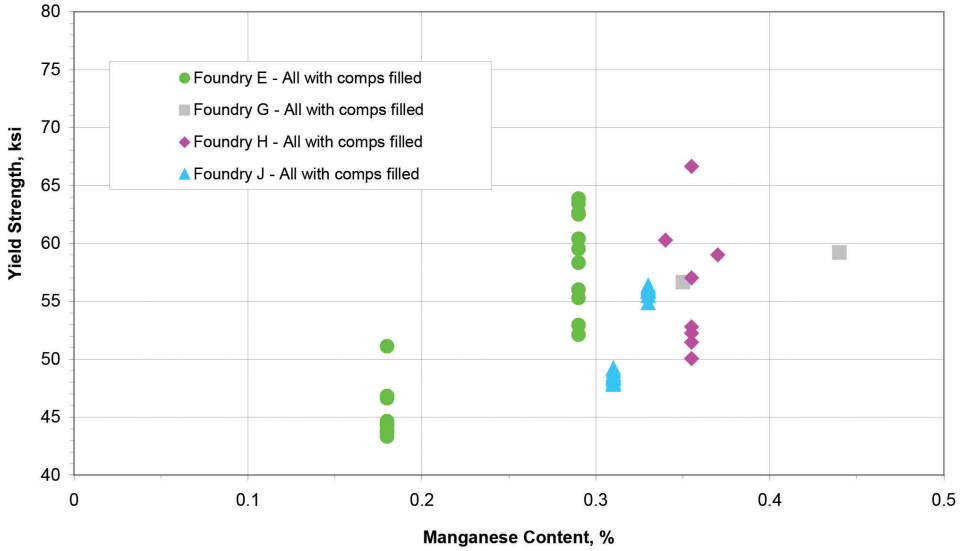


*Figure 12. Yield strength v. Manganese content for the 53 samples.*

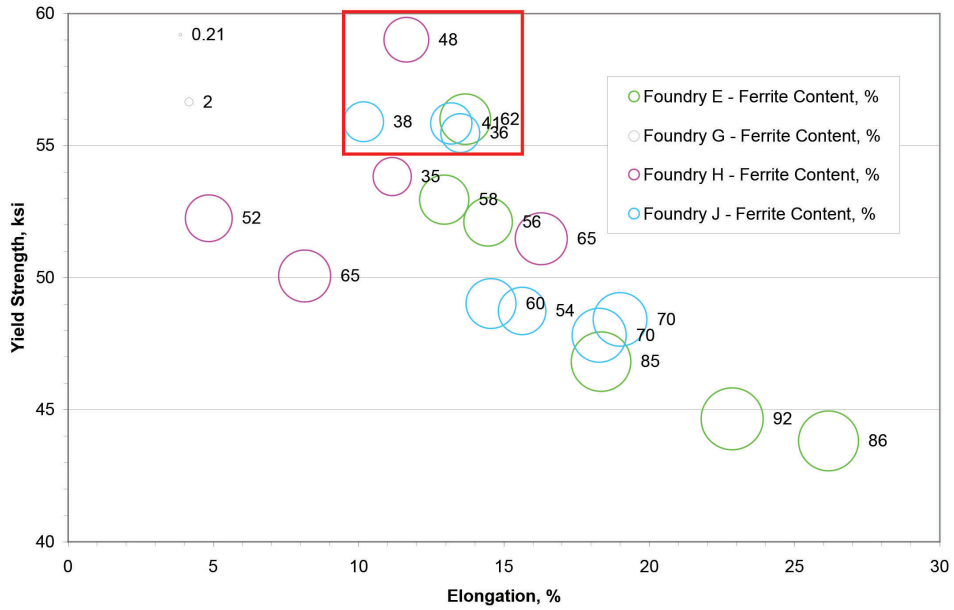


***Figure 13. Three dimensional plot showing elongation, yield strength and ferrite content (shown in the plot legend and next to the plotted points). The diameter of the circular "bubble" is proportional to the ferrite content. The points inside the red square indicate the "ideal ferrite" content of about 40 to 60% for achieving the target combination of ≥55 ksi yield strength and ≥10% elongation.***

Silicon and carbon equivalent also positively influence toughness. However, some of the elements that contribute to increasing the strength and strain hardening exponent seem to detract from toughness, namely (in decreasing order) manganese, manganese + copper, and copper. This observation stands to reason since these elements are also known to increase pearlite and strength.[21]

## Fracture Path Considerations

Additional observations are in order, particularly because of the differences that were observed for samples that seemingly had the same microstructure and yet had significantly different properties. Table 13 shows data for four samples that meet the strength requirements for Grade 80-55-06 but had significantly different ferrite contents, and different but relatively high elongation.

The principal investigators anticipated that the amount and distribution of the ferrite and pearlite constituents might provide some insight as to the microstructural characteristics that enhance the mechanical properties. The four castings contained levels of pearlite ranging from 38% to 68%, and yet all four met the specified properties of this grade of iron. The microstructures of these four castings are shown in Figures 14 to 17.

Some of the properties reported in Table 9 are as expected and some are unexpected. The higher the pearlite content the higher the tensile strength and yield strength. However, it was unexpected that a casting (#13) with only 38% pearlite would produce sufficient yield strength and tensile strength for this grade of ductile iron.

The difference in the properties of castings #15 and #52 were somewhat surprising. The two castings have essentially the same pearlite content; however, casting #15 has both higher strength and ductility. When comparing the microstructures of these two castings, some differences are apparent. In particular, the ferrite colonies in casting #15 are less continuous than in casting #52, where the ferrite extended from nodule to nodule. Multiple red lines have been superimposed on the micrograph in Figure 15 to illustrate the continuity of the ferrite colonies in casting #52. These lines pass through many graphite nodules without crossing into a pearlite region. As shown by the single red line in Figure 17 for casting #15, the ferrite colonies are more discrete with pearlite display-

***Table 9. Specific Structure-Property Information for Four Selected Samples***

| Sample ID | Nodularity (%) | Nodule Count ($mm^{-2}$) | Pearlite Content (%) | Yield Strength (ksi) | Tensile Strength (ksi) | Elongation (%) |
|---|---|---|---|---|---|---|
| **11** | 93.9 | 144 | 68 | 63.4 | 109 | 10.0 |
| **15** | 95.7 | 160 | 61 | 62.6 | 104 | 13.3 |
| **52** | 98.4 | 214 | 62 | 55.9 | 93 | 10.2 |
| **13** | 97.1 | 184 | 38 | 56.0 | 92 | 13.7 |
| ***D5506*** | ***Not Specified*** | | | ***55*** | ***80*** | ***6*** |

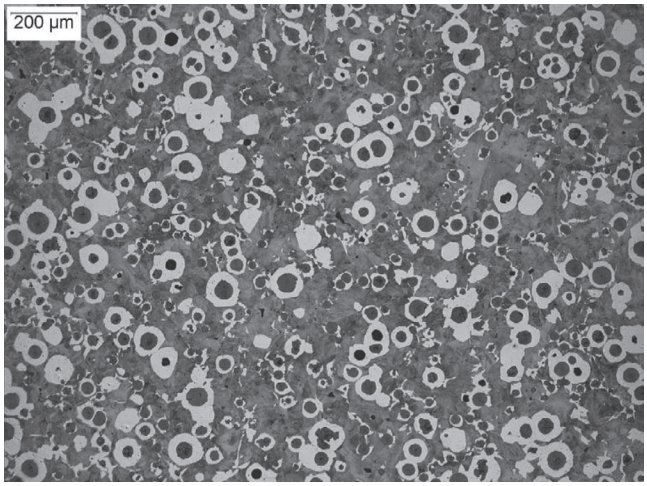


***Figure 14. Optical micrograph showing the matrix structure for sample 11.***

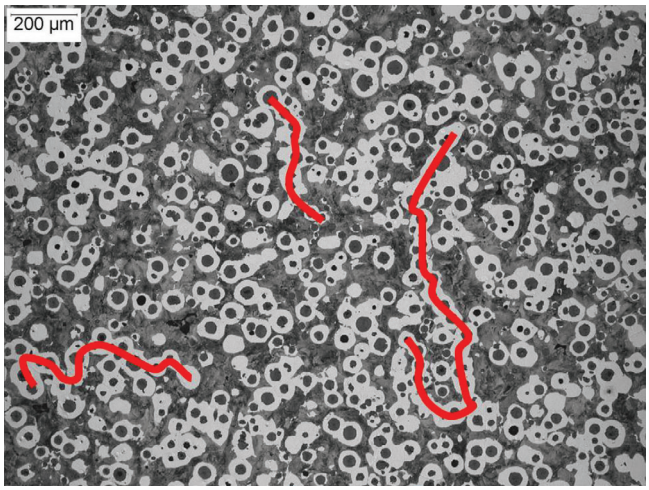


***Figure 16. Optical micrograph showing the matrix structure for sample 52.***

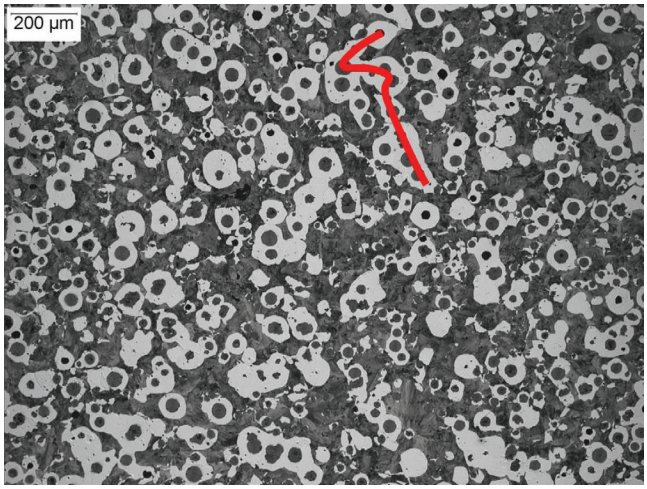


***Figure 15. Optical micrograph showing the matrix structure for sample 15.***

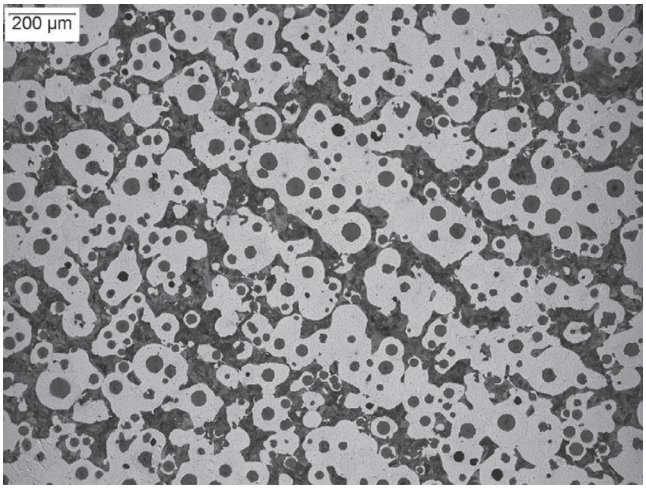


***Figure 17. Optical micrograph showing the matrix structure for sample 13.***

ing more continuity than the ferrite phase. The differences in nodule count may have contributed to this characteristic, where higher nodule count caused a greater continuity in the ferrite phase due to the shorter mean-free path between nodules. Tendencies for nodule alignment might also favor this ferrite distribution.

Certainly, as the ferrite content is diminished, the continuity of the ferrite phase will be reduced. This is readily apparent in the microstructure of casting #11, see Figure 14, where the somewhat lower ferrite content resulted in many more discrete ferrite colonies – most colonies contain only one or two nodules.

The authors propose the following mechanism to explain this ferrite morphology formation:

- Some nodules nucleate austenite and are incorporated into the growing dendrite
- Some nodules form late and are interdendritic
- Alloys segregates during dendrite growth
- The dendrite core is rich in Si and poor in Mn
- The dendrite core favors proeutectoid ferrite

Table 13 shows some expected properties. For example, higher pearlite content promoted higher yield and ultimate tensile strengths. Table 9 shows some properties that were unexpected because casting #13 with only 38% pearlite produced sufficient yield and ultimate tensile strength.

The principal investigators believe that the differences in yield strength and tensile strength, shown in Table 9 between castings #15 and #52, are related to differences in the continuity of the ferrite phase; namely, when the ferrite is continuous, as in casting #52, the continuity decreases the strength and elongation. When compared to casting #52, the ferrite is more randomly distributed and there is greater continuity of the pearlite in casting #15. The opposite is true for casting #52. The ferrite colonies in casting #15 are less continuous than in casting #52, where the ferrite extended from nodule-to-nodule, and the discontinuous ferrite in casting #15 promoted both higher strength and ductility.

Figures 18 and 19 show the following progress of cracking in a tensile test:

1. The ferrite phase yields around nodules
2. Voids form between the nodule and the metallic matrix
3. Voids in neighboring ferrite grains merge
4. Low strain-hardening in ferrite phase increases the stress on the pearlitic constituents
5. Eventually, pearlite becomes overstressed and transgranular cracks occur in the pearlite
6. These pearlite cracks become too large to sustain the load
7. Fast (transgranular cleavage) fracture occurs in the remaining metal ligaments

Figure 20 shows that the continuous ferrite decreases both strength and elongation.

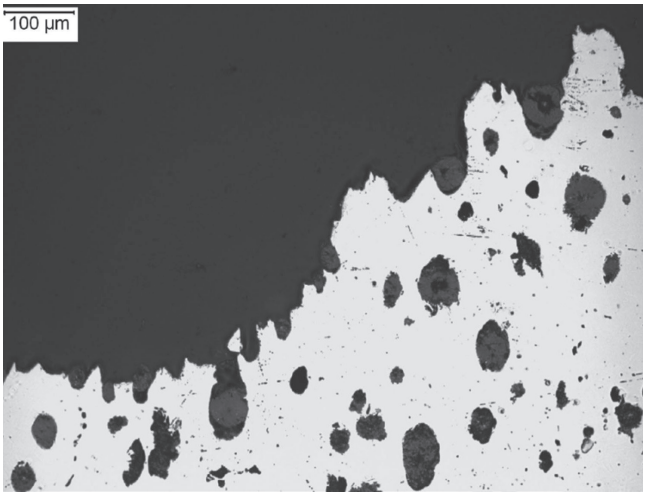


***Figure 18. Optical micrograph showing ductile tearing and microvoid coalescence in the ferrite grains of a tensile specimen from sample 4.***

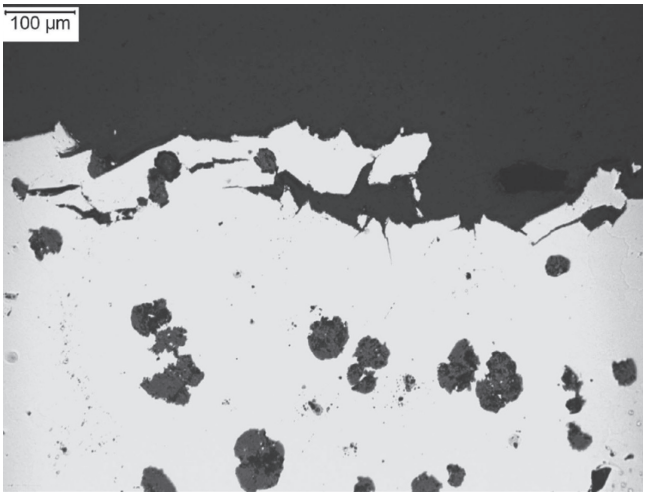


***Figure 19. Optical micrograph showing transgranular cleavage fracture at and below the tensile fracture face of a tensile specimen from sample 22.***

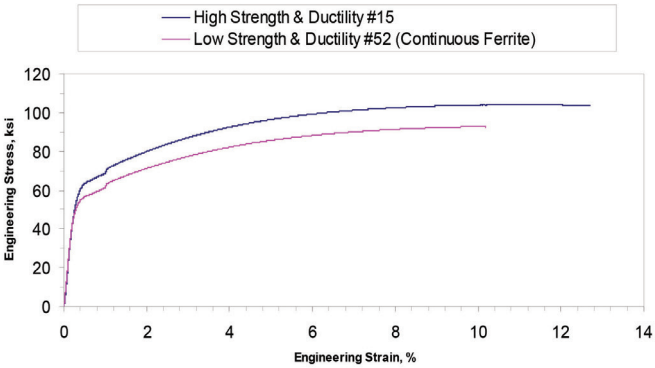


***Figure 20. Stress-strain curves for two samples with differing amounts of continuous ferrite. The continuous ferrite decreases both strength and ductility.***

These observations are very similar to those of earlier investigators[10,22] who found that 0.2% offset yield strength decreased linearly with the log of the mean free ferrite path in hypoeutectoid, eutectoid, spheroidized steels. The principal investigators believe that the microstructural differences are responsible for the differences in mechanical properties. Further work to determine the cause for ferrite colony formation to further maximize mechanical properties is worthy of consideration.

Other less obvious issues are important in this discussion of results, particularly as they influence strain hardening and toughness. Strain hardening exponent decreased with increasing ferrite content.[5,7] Toughness decreased and tensile strength increased with increasing strain hardening exponent.[5,7]

The principal investigators believe that increasing the strain hardening exponent (n) and toughness, as measured by either the area under the stress-strain curve (UT) or the further increase in strength beyond the onset of yielding, are two properties that can serve as metrics for examining the optimization of strength and ductility.

Optimizing ferrite content and reducing the continuity of ferrite colonies, as well as decreasing the n-value may prove useful for employing ductile iron in new applications that require high toughness. Lower nodule count and avoiding nodule alignment will most likely produce less connection of ferrite grains.

For the elements that were evaluated at sufficiently different levels, the correlation matrix indicates that the strain hardening exponent (n) is strongly and negatively influenced by increasing silicon content (and increasing carbon equivalent). The n-value is strongly and positively influenced by increasing contents of the following elements in decreasing order: copper + manganese, copper, and manganese.

### Correlations Between Literature, Substructure, and Mechanical Properties

The authors of reference 15 found that both the tensile strength and the ductility increased when the tensile loading was parallel to dendrites. This was explained by the presence of higher measured solute concentrations in the interdendritic region and the fact that ferrite formed in bands along the austenite dendrite center. This observation is somewhat consistent with the authors' observation that ferrite colony continuity reduced the strength and ductility of samples with nominally the same ferrite content.

Although the reviewed literature found that grain size reduction increased the strength of some irons, the effect was not pronounced unless heat treatment[19] was involved. The authors of this paper also found that the ferrite grain size did not influence the strength-ductility balance (e.g., see Figure 8) in the as-cast condition.

## Procedures and Results for Experimental Castings Research

### Motivation

Based on the results of the commercial foundry data survey, the principal investigators initiated subsequent research to study castings that were poured at a single experimental foundry and with a DOE methodology. The intent of this research was to more explicitly identify the relationship between yield strength above 55 ksi and elongation above 12% with the elements copper, manganese, and silicon. Other variables in the DOE program included inoculation and section size, and one selected condition was cast at a different commercial foundry for verification purposes. Finally, post-solidification heat-treatment trials were conducted to study the effect of heat treatment on the strength-ductility balance.

### Casting Procedures

The principal investigators worked with a sponsor foundry to develop a DOE for this second phase. This sponsor also agreed to conduct the melting, molding, and pouring that was required. The procedures are summarized in this paper. Full descriptions of the casting procedure are contained in References 6 and 7.

A total of nine heats of iron were cast, varying the Cu, Mn, and Si contents as shown in Table 10. Section size (1 in. versus 3 in.) and ladle versus ladle+in-stream inoculation were additional DOE variables.

All casting procedures were designed and monitored such that the metal in each test casting was produced as identically as possible. A common pouring basin was designed so that three Y-blocks could be poured at one time, in either 1 in. or 3 in. Y-block molds.

The participating foundry cut each Y-block to obtain 1 x 1-in. bars for the 1-in. Y-blocks and 1 x 3-in. slabs for the 3-in. Y-blocks prior to shipment to the principal investigators' laboratory. The heats were magnesium treated using

***Table 10. Nominal Elemental Content Variation in the Design of Experiments (Each heat also had a section size and inoculation variation)***

| DOE Condition # | Heat # | Copper (wt%) | Manganese (wt%) | Silicon (wt%) | Cu | Mn | Si |
|---|---|---|---|---|---|---|---|
| 1 | 1 | 0.3 | 0.2 | 2.4 | - | - | - |
| 2 | 2 | 0.3 | 0.2 | 2.8 | - | - | + |
| 3 | 3 | 0.3 | 0.4 | 2.4 | - | + | - |
| 4 | 4 | 0.3 | 0.5 | 2.8 | - | + | + |
| 5 | 5 | 0.6 | 0.2 | 2.2 | + | - | - |
| 6 | 6 | 0.6 | 0.3 | 2.6 | + | - | + |
| 7 | 7 | 0.6 | 0.4 | 2.4 | + | + | - |
| 8 | 11 | 0.6 | 0.4 | 2.7 | + | + | + |
| 8 (repeat) | 12 | 0.6 | 0.3 | 2.5 | + | + | + |

the sandwich technique. Once treated, the iron was transferred to a pouring ladle, inoculated, and the slag removed. Tapping and pouring temperatures were similar among the nine heats and recorded for each heat; these temperatures respectively averaged 1,524 and 1,380C (2,776 and 2,516F). The shakeout time for all molds was "overnight" to eliminate any shakeout time variation. A "catsup cup" was used to hold a "pinch" of inoculant to perform the in-stream inoculant requirement.

Each heat poured two molds with three 1-in.Y-block cavities and two molds with three 3-in. Y-block cavities. Three of the 1-in.Y-blocks and three of the 3-in.Y-blocks were poured with ladle inoculation alone. The other three 1-in. Y-blocks and three 3-in. Y-blocks were poured with ladle plus stream inoculation. Each heat represented one of the DOE composition variations. This process yielded three Y-blocks of each section size for each DOE condition.

### Design of Experiments Methodology

The DOE required eight individual heats of iron covering all the chemistry combinations shown in Table 10. The elemental contents are actually measured values in that table, but with low precision rounding to foster easier comparison of the low and high values for each DOE alloying element variable. The low and high levels of each of the DOE alloying element levels are indicated with minus (-) and plus (+) signs, respectively. In some respects, some of the compositions were slightly off target, as indicated in red, but the DOE methodology and results were not significantly affected. One additional heat of the high copper, manganese, and silicon contents was poured for a repeatability check.

### Metallography and Chemical Analysis

Chemical analysis was conducted on the samples in such a way that all of the heats cast were analyzed in multiples. At least four compositions per heat and at least two compositions for each inoculation method and section size were analyzed. For Heats 1 and 2, significantly more compositions were determined.

The carbon and sulfur contents were determined combustometrically (LECO or ASTM E1019), and glow discharge optical emission spectroscopy (GD-OES) was used to determine all other elemental contents. Table 11 shows the chemical analyses measured by the authors.

Multiple transverse metallographic samples were obtained from tensile blanks for each heat. At least four samples were tested for each heat and at least two metallographic samples were analyzed for each inoculation method and section size. For Heats 1 and 2, significantly more metallographic samples were obtained and analyzed.

All samples were mounted, polished, and etched in accordance with ASTM E3. Ferrite content, nodule count and nodularity were determined by image analysis in accordance with ASTM A247 and E1245.

### Mechanical Testing

The principal investigators tested triplicate tensile samples from various positions in selected Y-block locations for Heats 1 and 2. For the other heats, duplicate samples were tested for each combination of section size and inoculation method. Tensile properties were determined in accordance with ASTM E8 and Brinell hardness was determined in accordance with ASTM E10. Brinell hardness was measured on 56 samples using a 3,000-kg load and a 10mm diameter tungsten carbide ball. All tensile samples utilized a standard 0.505 in. diameter by 2 in. gauge length tensile bar. The same tensile properties that were measured in the earlier foundry data assessment, as discussed earlier in this paper, were measured in this section of the study.

### Test Bar Location

Since it was anticipated that properties might vary with test bar location, the optimum test bar location was determined by testing samples from multiple locations in one of the 1-in. Y-Blocks and in one of the 3-in.Y-Blocks from Heat #2, which were poured with ladle inoculation only. These bars were mechanically tested and metallographic samples from the test bars were evaluated. The purpose for this testing was to compare the properties from the different locations in the Y-blocks and determine where to take the test bars for the DOE comparison for the rest of the study. The bottom location was selected for the 1-in.Y-blocks and the middle-middle location was selected for the 3-in.Y-blocks.

### Data Sets

Tables 11, 12, and 13 show the results obtained for all the DOE conditions. Each mechanical property result in Table 16 represents the average of three tests for each DOE condition for Heats 1 and 2, and the average of two tests for all the other heats. The compositions and metallographic results in Tables 11 and 13 are not averages. The ranges of duplicate and triplicate values were relatively tight in the multiple measurements; therefore, the statistical analyses were conducted without requiring the complexity of "missing data" routines in the statistical analyses. The individual test results are contained in Reference 6.

### Comparison of Commercial Foundry Data with Experimental Castings Results

Figure 21 shows a correlation of selected mechanical properties from this experimental castings study. The data are plotted versus the results for different foundries from the Commercial Foundry Data Survey. Generally good agreement was obtained between the experimental castings prop-

### Table 11. Chemical Analysis of Experimental Castings, wt%

| Overall Sample # | Cast Section Size | DOE Condition # | Heat # | Mold | Inoculation | C | S | P | Si | Mn | Cr | Ni | Mo | V | Al | Cu | Mg | Ti | Sb | Ce | Sn |
|---|---|---|---|---|---|---|---|---|---|---|---|---|---|---|---|---|---|---|---|---|---|
| 1 | 1" | 1 | 1 | 1 | In-Ladle Only | 3.54 | 0.008 | 0.029 | 2.31 | 0.18 | 0.04 | 0.02 | <0.01 | 0.0120 | 0.0090 | 0.28 | 0.053 | 0.008 | <0.005 | 0.0120 | <0.005 |
| 4 | 1" | | | 2 | In-Ladle & In-Stream | 3.55 | 0.009 | 0.028 | 2.44 | 0.18 | 0.05 | 0.02 | <0.01 | 0.0090 | 0.0100 | 0.28 | 0.051 | 0.008 | <0.005 | 0.0110 | <0.005 |
| 7 | 3" | | | 3 | In-Ladle Only | 3.54 | 0.008 | 0.031 | 2.30 | 0.17 | 0.05 | 0.02 | <0.01 | 0.0110 | 0.0090 | 0.28 | 0.049 | 0.008 | <0.005 | 0.0120 | <0.005 |
| 11 | 3" | | | 4 | In-Ladle & In-Stream | 3.54 | 0.008 | 0.029 | 2.56 | 0.17 | 0.05 | 0.02 | <0.01 | 0.0090 | 0.0110 | 0.28 | 0.047 | 0.007 | <0.005 | 0.0110 | <0.005 |
| 15 | 1" | 2 | 2 | 1 | In-Ladle Only | 3.48 | 0.007 | 0.029 | 2.72 | 0.18 | 0.05 | 0.02 | <0.01 | 0.0110 | 0.0080 | 0.29 | 0.038 | 0.008 | <0.005 | 0.0110 | <0.005 |
| 20 | 1" | | | 2 | In-Ladle & In-Stream | 3.48 | 0.007 | 0.030 | 2.75 | 0.18 | 0.05 | 0.02 | <0.01 | 0.0100 | 0.0080 | 0.28 | 0.038 | 0.008 | <0.005 | 0.0100 | <0.005 |
| 23 | 3" | | | 3 | In-Ladle Only | 3.49 | 0.007 | 0.030 | 2.84 | 0.17 | 0.05 | 0.02 | <0.01 | 0.0100 | 0.0090 | 0.28 | 0.037 | 0.007 | <0.005 | 0.0130 | <0.005 |
| 31 | 3" | | | 4 | In-Ladle & In-Stream | 3.48 | 0.007 | 0.030 | 2.73 | 0.17 | 0.05 | 0.02 | <0.01 | 0.0100 | 0.0080 | 0.28 | 0.038 | 0.008 | <0.005 | 0.0120 | <0.005 |
| 34 | 1" | 3 | 3 | 1 | In-Ladle Only | 3.64 | <0.005 | 0.030 | 2.37 | 0.44 | 0.05 | 0.02 | <0.01 | 0.01 | 0.011 | 0.29 | 0.054 | 0.007 | <0.005 | 0.006 | <0.005 |
| 36 | 1" | | | 2 | In-Ladle & In-Stream | 3.63 | <0.005 | 0.031 | 2.41 | 0.43 | 0.05 | 0.02 | <0.01 | 0.012 | 0.011 | 0.29 | 0.055 | 0.008 | <0.005 | 0.004 | <0.005 |
| 38 | 3" | | | 3 | In-Ladle Only | 3.61 | <0.005 | 0.032 | 2.35 | 0.43 | 0.05 | 0.02 | <0.01 | 0.011 | 0.010 | 0.29 | 0.054 | 0.007 | <0.005 | 0.007 | <0.005 |
| 40 | 3" | | | 4 | In-Ladle & In-Stream | 3.57 | <0.005 | 0.032 | 2.45 | 0.43 | 0.05 | 0.02 | <0.01 | 0.011 | 0.011 | 0.29 | 0.052 | 0.007 | <0.005 | 0.007 | <0.005 |
| 42 | 1" | 4 | 4 | 1 | In-Ladle Only | 3.53 | 0.005 | 0.030 | 2.75 | 0.43 | 0.04 | 0.02 | <0.01 | 0.012 | 0.007 | 0.29 | 0.048 | 0.009 | <0.005 | 0.012 | <0.005 |
| 44 | 1" | | | 2 | In-Ladle & In-Stream | 3.56 | 0.005 | 0.031 | 2.87 | 0.45 | 0.04 | 0.02 | <0.01 | 0.007 | 0.011 | 0.29 | 0.047 | 0.009 | <0.005 | 0.01 | <0.005 |
| 46 | 3" | | | 3 | In-Ladle Only | 3.55 | <0.005 | 0.030 | 2.76 | 0.42 | 0.04 | 0.02 | <0.01 | 0.006 | 0.01 | 0.29 | 0.047 | 0.009 | <0.005 | 0.011 | <0.005 |
| 48 | 3" | | | 4 | In-Ladle & In-Stream | 3.50 | <0.005 | 0.026 | 2.90 | 0.42 | 0.04 | 0.02 | <0.01 | 0.005 | 0.011 | 0.29 | 0.041 | 0.007 | <0.005 | 0.01 | <0.005 |
| 50 | 1" | 5 | 5 | 1 | In-Ladle Only | 3.54 | <0.005 | 0.028 | 2.21 | 0.21 | 0.04 | 0.02 | <0.01 | 0.006 | 0.009 | 0.60 | 0.044 | 0.008 | <0.005 | 0.009 | <0.005 |
| 52 | 1" | | | 2 | In-Ladle & In-Stream | 3.52 | 0.005 | 0.028 | 2.30 | 0.21 | 0.04 | 0.02 | <0.01 | 0.007 | 0.009 | 0.60 | 0.042 | 0.008 | <0.005 | 0.008 | <0.005 |
| 54 | 3" | | | 3 | In-Ladle Only | 3.54 | <0.005 | 0.027 | 2.22 | 0.21 | 0.04 | 0.02 | <0.01 | 0.005 | 0.009 | 0.59 | 0.042 | 0.007 | <0.005 | 0.007 | <0.005 |
| 56 | 3" | | | 4 | In-Ladle & In-Stream | 3.51 | <0.005 | 0.029 | 2.26 | 0.21 | 0.04 | 0.02 | <0.01 | 0.006 | 0.009 | 0.60 | 0.043 | 0.008 | <0.005 | 0.008 | <0.005 |
| 58 | 1" | 6 | 6 | 1 | In-Ladle & In-Stream | 3.52 | <0.005 | 0.031 | 2.59 | 0.28 | 0.04 | 0.02 | <0.01 | 0.006 | 0.008 | 0.56 | 0.045 | 0.01 | <0.005 | 0.007 | <0.005 |
| 60 | 1" | | | 2 | In-Ladle Only | 3.49 | <0.005 | 0.029 | 2.71 | 0.28 | 0.04 | 0.02 | <0.01 | 0.006 | 0.009 | 0.57 | 0.04 | 0.01 | <0.005 | 0.01 | <0.005 |
| 62 | 3" | | | 3 | In-Ladle & In-Stream | 3.45 | <0.005 | 0.029 | 2.60 | 0.28 | 0.04 | 0.02 | <0.01 | 0.006 | 0.008 | 0.56 | 0.044 | 0.01 | <0.005 | 0.011 | <0.005 |
| 64 | 3" | | | 4 | In-Ladle Only | 3.47 | <0.005 | 0.031 | 2.68 | 0.28 | 0.04 | 0.02 | <0.01 | 0.007 | 0.009 | 0.56 | 0.047 | 0.012 | <0.005 | 0.008 | <0.005 |
| 66 | 1" | 7 | 7 | 1 | In-Ladle & In-Stream | 3.51 | <0.005 | 0.029 | 2.28 | 0.41 | 0.04 | 0.02 | <0.01 | 0.006 | 0.010 | 0.58 | 0.049 | 0.008 | <0.005 | 0.012 | <0.005 |
| 68 | 1" | | | 2 | In-Ladle Only | 3.52 | <0.005 | 0.030 | 2.45 | 0.40 | 0.04 | 0.02 | <0.01 | 0.006 | 0.011 | 0.59 | 0.046 | 0.007 | <0.005 | 0.008 | <0.005 |
| 70 | 3" | | | 3 | In-Ladle & In-Stream | 3.51 | <0.005 | 0.030 | 2.30 | 0.40 | 0.04 | 0.02 | <0.01 | 0.007 | 0.010 | 0.58 | 0.047 | 0.008 | <0.005 | 0.01 | <0.005 |
| 72 | 3" | | | 4 | In-Ladle Only | 3.47 | <0.005 | 0.030 | 2.44 | 0.40 | 0.04 | 0.02 | <0.01 | 0.007 | 0.011 | 0.59 | 0.044 | 0.007 | <0.005 | 0.008 | <0.005 |
| 74 | 1" | 8 | 11 | 1 | In-Ladle & In-Stream | 3.50 | 0.010 | 0.030 | 2.69 | 0.41 | 0.06 | 0.02 | <0.01 | 0.011 | 0.009 | 0.60 | 0.040 | 0.011 | <0.005 | 0.009 | <0.005 |
| 76 | 1" | | | 2 | In-Ladle Only | 3.50 | 0.012 | 0.032 | 2.62 | 0.41 | 0.06 | 0.02 | <0.01 | 0.010 | 0.008 | 0.59 | 0.041 | 0.011 | <0.005 | 0.015 | <0.005 |
| 78 | 3" | | | 3 | In-Ladle & In-Stream | 3.47 | 0.011 | 0.032 | 2.77 | 0.40 | 0.06 | 0.02 | <0.01 | 0.012 | 0.009 | 0.59 | 0.041 | 0.011 | <0.005 | 0.009 | <0.005 |
| 80 | 3" | | | 4 | In-Ladle Only | 3.45 | 0.011 | 0.031 | 2.63 | 0.40 | 0.06 | 0.02 | <0.01 | 0.009 | 0.008 | 0.60 | 0.042 | 0.010 | <0.005 | 0.013 | <0.005 |
| 82 | 1" | 8 | 12 | 1 | In-Ladle & In-Stream | 3.41 | 0.012 | 0.028 | 2.56 | 0.32 | 0.06 | 0.02 | <0.01 | 0.009 | 0.008 | 0.59 | 0.040 | 0.010 | <0.005 | 0.009 | <0.005 |
| 84 | 1" | | | 2 | In-Ladle Only | 3.38 | 0.012 | 0.029 | 2.51 | 0.31 | 0.06 | 0.02 | <0.01 | 0.009 | 0.007 | 0.58 | 0.039 | 0.010 | <0.005 | 0.009 | <0.005 |
| 86 | 1" | | | 3 | In-Ladle & In-Stream | 3.36 | 0.010 | 0.026 | 2.58 | 0.31 | 0.06 | 0.02 | <0.01 | 0.009 | 0.008 | 0.58 | 0.037 | 0.009 | <0.005 | 0.010 | <0.005 |
| 88 | 1" | | | 4 | In-Ladle Only | 3.31 | 0.011 | 0.028 | 2.52 | 0.31 | 0.06 | 0.02 | <0.01 | 0.009 | 0.007 | 0.58 | 0.039 | 0.010 | <0.005 | 0.008 | <0.005 |

### Table 12. Average Mechanical Property Results Obtained for all the DOE Conditions

| Average Sample No. | DOE Condition # | Heat # | Cast Section Size | Mold | Inoculation | Brinell Hardness | UTS (ksi) | YS (ksi) | %El at Fracture | %RA | % Elong. | Uniform Elongation (%) | Strain Hardening (SH), (%) | Toughness, UT (ksi-in/in) |
|---|---|---|---|---|---|---|---|---|---|---|---|---|---|---|
| 1 | 1 | 1 | 1" | 1 | In-Ladle Only | 191 | 81.2 | 47.0 | 14.8 | 13.3 | 15.1 | 13.9 | 72.8 | 9.7 |
| 2 | | | 1" | 2 | In-Ladle & In-Stream | 179 | 77.9 | 45.7 | 16.4 | 15.9 | 16.7 | 13.3 | 70.4 | 10.3 |
| 3 | | | 3" | 3 | In-Ladle Only | 179 | 79.0 | 43.0 | 13.6 | 12.0 | 14.6 | 12.3 | 83.8 | 8.9 |
| 4 | | | 3" | 4 | In-Ladle & In-Stream | 173 | 73.3 | 43.0 | 14.5 | 12.6 | 15.3 | 13.0 | 70.5 | 8.9 |
| 5 | 2 | 2 | 1" | 1 | In-Ladle Only | 164 | 68.8 | 45.0 | 22.2 | 25.4 | 22.4 | 16.3 | 53.0 | 12.8 |
| 6 | | | 1" | 2 | In-Ladle & In-Stream | 161 | 67.6 | 45.0 | 19.5 | 23.2 | 23.3 | 13.8 | 50.0 | 13.1 |
| 7 | | | 3" | 3 | In-Ladle Only | 152 | 65.3 | 42.6 | 21.1 | 24.0 | 21.9 | 15.8 | 53.4 | 11.8 |
| 8 | | | 3" | 4 | In-Ladle & In-Stream | 156 | 64.4 | 44.4 | 21.2 | 20.3 | 21.0 | 15.8 | 44.8 | 11.4 |
| 9 | 3 | 3 | 1" | 1 | In-Ladle Only | 218 | 96.8 | 53.3 | 12.1 | 9.7 | 11.8 | 11.4 | 81.4 | 8.8 |
| 10 | | | 1" | 2 | In-Ladle & In-Stream | 210 | 93.9 | 52.6 | 13.6 | 11.8 | 13.3 | 11.7 | 78.5 | 9.8 |
| 11 | | | 3" | 3 | In-Ladle Only | 210 | 88.3 | 49.0 | 6.7 | 4.9 | 6.7 | 6.7 | 80.2 | 4.6 |
| 12 | | | 3" | 4 | In-Ladle & In-Stream | 207 | 89.7 | 49.9 | 8.4 | 6.5 | 8.4 | 8.4 | 79.6 | 5.8 |
| 13 | 4 | 4 | 1" | 1 | In-Ladle Only | 201 | 88.9 | 53.1 | 14.3 | 12.3 | 13.8 | 12.3 | 67.4 | 9.8 |
| 14 | | | 1" | 2 | In-Ladle & In-Stream | 198 | 85.8 | 53.4 | 16.5 | 15.5 | 16.4 | 13.4 | 60.5 | 11.4 |
| 15 | | | 3" | 3 | In-Ladle Only | 201 | 86.5 | 51.2 | 11.2 | 8.5 | 11.3 | 10.8 | 68.8 | 7.8 |
| 16 | | | 3" | 4 | In-Ladle & In-Stream | 197 | 85.4 | 52.5 | 11.9 | 9.6 | 11.9 | 11.4 | 62.7 | 8.2 |
| 17 | 5 | 5 | 1" | 1 | In-Ladle Only | 213 | 94.1 | 53.5 | 11.1 | 9.2 | 10.9 | 10.2 | 75.8 | 8.1 |
| 18 | | | 1" | 2 | In-Ladle & In-Stream | 243 | 112.1 | 60.5 | 9.6 | 7.5 | 9.1 | 9.4 | 85.1 | 7.8 |
| 19 | | | 3" | 3 | In-Ladle Only | 226 | 91.5 | 53.2 | 3.8 | 3.0 | 3.5 | 3.9 | 72.2 | 2.5 |
| 20 | | | 3" | 4 | In-Ladle & In-Stream | 226 | 97.5 | 53.8 | 5.5 | 4.0 | 5.7 | 5.5 | 81.1 | 4.3 |
| 21 | 6 | 6 | 1" | 1 | In-Ladle & In-Stream | 245 | 109.0 | 62.6 | 6.4 | 5.0 | 5.8 | 6.5 | 74.0 | 5.0 |
| 22 | | | 1" | 2 | In-Ladle Only | 246 | 112.7 | 64.1 | 10.5 | 8.1 | 10.4 | 10.2 | 75.8 | 9.2 |
| 23 | | | 3" | 3 | In-Ladle & In-Stream | 227 | 87.5 | 56.7 | 3.2 | 2.5 | 3.0 | 3.2 | 54.3 | 2.2 |
| 24 | | | 3" | 4 | In-Ladle Only | 228 | 94.2 | 57.9 | 5.2 | 4.1 | 5.0 | 5.2 | 62.8 | 3.8 |
| 25 | 7 | 7 | 1" | 1 | In-Ladle & In-Stream | 244 | 113.8 | 61.8 | 6.9 | 5.3 | 6.8 | 6.9 | 84.2 | 5.9 |
| 26 | | | 1" | 2 | In-Ladle Only | 247 | 113.5 | 63.3 | 7.6 | 5.8 | 7.3 | 7.7 | 79.4 | 6.4 |
| 27 | | | 3" | 3 | In-Ladle & In-Stream | 227 | 92.9 | 53.8 | 4.0 | 3.0 | 3.7 | 4.0 | 72.6 | 2.7 |
| 28 | | | 3" | 4 | In-Ladle Only | 228 | 91.2 | 55.7 | 3.6 | 3.2 | 3.5 | 3.7 | 63.8 | 2.6 |
| 29 | 8 | 11 | 1" | 1 | In-Ladle & In-Stream | 248 | 112.2 | 65.1 | 9.9 | 7.7 | 9.3 | 9.8 | 72.2 | 8.3 |
| 30 | | | 1" | 2 | In-Ladle Only | 251 | 112.6 | 65.0 | 8.9 | 7.0 | 8.5 | 8.9 | 73.3 | 7.6 |
| 31 | | | 3" | 3 | In-Ladle & In-Stream | 233 | 86.4 | 59.2 | 3.3 | 2.6 | 3.3 | 3.3 | 46.1 | 2.4 |
| 32 | | | 3" | 4 | In-Ladle Only | 234 | 87.5 | 58.8 | 2.9 | 2.4 | 3.3 | 2.9 | 48.9 | 2.4 |
| 33 | 8 | 12 | 1" | 1 | In-Ladle & In-Stream | 244 | 110.6 | 62.8 | 9.7 | 7.4 | 8.8 | 9.7 | 76.0 | 7.6 |
| 34 | | | 1" | 2 | In-Ladle Only | 245 | 111.1 | 62.4 | 9.8 | 7.5 | 9.2 | 9.9 | 77.9 | 8.0 |
| 35 | | | 3" | 3 | In-Ladle & In-Stream | 225 | 91.7 | 56.5 | 5.0 | 4.5 | 4.0 | 5.0 | 62.4 | 2.9 |
| 36 | | | 3" | 4 | In-Ladle Only | 231 | 85.9 | 56.4 | 2.8 | 2.4 | 3.0 | 2.9 | 52.4 | 2.1 |

erties and those from the commercial foundries. Heats 4, 5, 6, 7 and 11 from the experimental castings study exhibited properties approaching the desired properties in Grade D5506, i.e., yield strength approaching 55 ksi, % elongation over 12% and ultimate tensile strength over 85 ksi, which is close to optimum in the commercial foundry survey.

Figure 22 plots one of the key mechanical property parameters versus ferrite content; correlations of the other key parameter variations with ferrite content are contained in References 6 and 7. As was found in the Commercial Foundry Data Survey, one of the other key parameters, i.e., the percent strain hardening (%SH as calculated in Equation 1) decreases with increasing ferrite content above 40%. However, the %SH is relatively constant with significant data scatter at ferrite contents below 40%.

## Data Repeatability

Through visual comparison of the duplicate and triplicate values, excellent mechanical property repeatability within each heat and the DOE test condition were obtained. For a repeatability check, one additional heat of the high copper and high manganese with high silicon condition was poured. Table 16 also shows that the mechanical properties for Heats 11 and 12 were very similar, although the strengths of Heat 12 were slightly lower than those of Heat 11, perhaps due to the lower Mn content of Heat 12 (see Tables 14 and 15). Hereafter, only the results from Heat 11 were used in the statistical analyses.

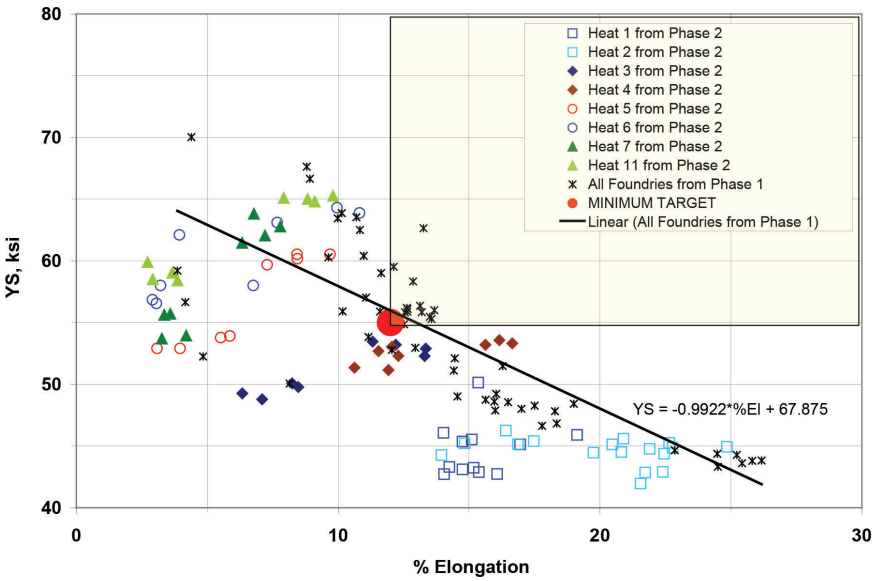


***Figure 21. Yield strength versus elongation for Phase 2 DOE results and Phase 1 results from commercial foundries. The shaded region shows the target properties.***

***Table 13. Average Microstructural Image Analysis Results Obtained for all the DOE Conditions***

| Average Sample No. | DOE Condition # | Heat # | Cast Section Size | Mold | Inoculation | Nodularity (%) | Nodule Count (mm$^{-2}$) | # of Class 7 (%) | # of Class 6 (%) | # of Class 5 (%) | # of Class 4 (%) | Maximum Nodule Size (µm) | Graphite Volume Fraction (%) | Mean Ferrite Volume Fraction (%) | Std Dev Ferrite Volume Fraction (%) |
|---|---|---|---|---|---|---|---|---|---|---|---|---|---|---|---|
| 1 | 1 | 1 | 1" | 1 | In-Ladle Only | 92.9 | 246.1 | 49.47 | 50.12 | 0.42 | 0 | 51.2 | 7.490 | 52.42 | 2.95 |
| 2 | | | 1" | 2 | In-Ladle & In-Stream | 96.9 | 264.5 | 45.52 | 53.15 | 1.33 | 0 | 52.7 | 9.230 | 61.91 | 2.19 |
| 3 | | | 3" | 3 | In-Ladle Only | 82.5 | 66.8 | 31.97 | 25.75 | 37 | 5.29 | 136.7 | 10.380 | 41.30 | 4.35 |
| 4 | | | 3" | 4 | In-Ladle & In-Stream | 91.6 | 73.1 | 14.47 | 41.95 | 41.95 | 1.63 | 110.6 | 8.780 | 52.79 | 5.59 |
| 5 | 2 | 2 | 1" | 1 | In-Ladle Only | 92.9 | 191.6 | 28.73 | 62 | 9 | 0 | 72 | 9.960 | 80.64 | 1.3 |
| 6 | | | 1" | 2 | In-Ladle & In-Stream | 94.6 | 255.3 | 47.1 | 51.89 | 1 | 0 | 56.2 | 8.790 | 92.33 | 1.13 |
| 7 | | | 3" | 3 | In-Ladle Only | 77.8 | 55.9 | 15.87 | 38.66 | 41.71 | 3.76 | 119.1 | 8.790 | 90.40 | 2.5 |
| 8 | | | 3" | 4 | In-Ladle & In-Stream | 89 | 110 | 16.71 | 59 | 24 | 0.16 | 93 | 9.740 | 76.23 | 1.15 |
| 9 | 3 | 3 | 1" | 1 | In-Ladle Only | 93.3 | 100.6 | 15.55 | 47.29 | 36.93 | 0.23 | 100.5 | 10.4 | 26.19 | 2.12 |
| 10 | | | 1" | 2 | In-Ladle & In-Stream | 92.6 | 113.3 | 16.27 | 52.46 | 31.17 | 0.1 | 81.2 | 10.39 | 26.01 | 2.09 |
| 11 | | | 3" | 3 | In-Ladle Only | 78.1 | 38.3 | 18.84 | 21.36 | 50.15 | 9.64 | 142.5 | 10.01 | 15.32 | 1.68 |
| 12 | | | 3" | 4 | In-Ladle & In-Stream | 86.9 | 60.2 | 16.82 | 28.26 | 51.04 | 3.88 | 133.1 | 10.39 | 27.07 | 4.09 |
| 13 | 4 | 4 | 1" | 1 | In-Ladle Only | 83.6 | 76.1 | 17.28 | 53.48 | 27.97 | 1.27 | 109.8 | 9.1 | 42.02 | 3.5 |
| 14 | | | 1" | 2 | In-Ladle & In-Stream | 96.4 | 187.9 | 27.91 | 62.58 | 9.48 | 0.03 | 82.8 | 9.89 | 51.21 | 2.48 |
| 15 | | | 3" | 3 | In-Ladle Only | 75.2 | 46.2 | 20.69 | 24.14 | 48.28 | 6.9 | 136.8 | 9.47 | 30.86 | 4.1 |
| 16 | | | 3" | 4 | In-Ladle & In-Stream | 82.3 | 59.8 | 15.89 | 32.25 | 47.76 | 4.09 | 136.7 | 10.05 | 37.47 | 6.16 |
| 17 | 5 | 5 | 1" | 1 | In-Ladle Only | 94.3 | 97.4 | 16.75 | 50.79 | 32.28 | 0.18 | 84.8 | 9.3 | 12.22 | 1.5 |
| 18 | | | 1" | 2 | In-Ladle & In-Stream | 95.6 | 145.3 | 24.78 | 61.86 | 13.35 | 0 | 66.6 | 8.34 | 8.15 | 0.816 |
| 19 | | | 3" | 3 | In-Ladle Only | 75.3 | 40.7 | 21.12 | 25.45 | 47.27 | 6.15 | 129.6 | 8.95 | 4.66 | 1.47 |
| 20 | | | 3" | 4 | In-Ladle & In-Stream | 88.7 | 50.3 | 18.53 | 25.88 | 50.28 | 5.31 | 125.6 | 8.65 | 2.84 | 0.683 |
| 21 | 6 | 6 | 1" | 1 | In-Ladle & In-Stream | 88.4 | 53.6 | 14.4 | 39.07 | 39.7 | 6.79 | 124.3 | 10.83 | 4.79 | 1.14 |
| 22 | | | 1" | 2 | In-Ladle Only | 96.5 | 168 | 30.41 | 58.79 | 10.8 | 0 | 70.6 | 8.9 | 15.01 | 1.31 |
| 23 | | | 3" | 3 | In-Ladle & In-Stream | 76 | 34.6 | 20.23 | 21.38 | 48.36 | 9.87 | 161.2 | 8.95 | 10.04 | 2.47 |
| 24 | | | 3" | 4 | In-Ladle Only | 82.2 | 39 | 17.81 | 21.9 | 50.66 | 9.64 | 131.7 | 9.05 | 12.22 | 1.81 |
| 25 | 7 | 7 | 1" | 1 | In-Ladle & In-Stream | 94.7 | 102.2 | 16.54 | 52.06 | 31.35 | 0.06 | 95.2 | 8.99 | 4.17 | 0.554 |
| 26 | | | 1" | 2 | In-Ladle Only | 94.2 | 110.9 | 17.8 | 55.77 | 26.37 | 0.05 | 84.6 | 8.75 | 7.612 | 1.25 |
| 27 | | | 3" | 3 | In-Ladle & In-Stream | 69.7 | 33.6 | 23.05 | 22.88 | 42.71 | 11.36 | 138.4 | 9.31 | 2.56 | 1.29 |
| 28 | | | 3" | 4 | In-Ladle Only | 86.3 | 44.5 | 17.62 | 23.12 | 53.13 | 6.13 | 119.2 | 8.31 | 2.53 | 1.28 |
| 29 | 8 | 11 | 1" | 1 | In-Ladle & In-Stream | 95 | 213.5 | 43.38 | 49.45 | 7.14 | 0.03 | 82.7 | 9.19 | 18.11 | 1.33 |
| 30 | | | 1" | 2 | In-Ladle Only | 91.3 | 128.1 | 24.6 | 52.09 | 23.22 | 0.09 | 89.9 | 9.78 | 14.75 | 0.975 |
| 31 | | | 3" | 3 | In-Ladle & In-Stream | 79.7 | 118.8 | 25.48 | 60.44 | 13.41 | 0.67 | 102.2 | 9.38 | 21.38 | 3.86 |
| 32 | | | 3" | 4 | In-Ladle Only | 85.4 | 53.4 | 29 | 21.54 | 43.07 | 6.4 | 149.6 | 9.98 | 8.58 | 2.39 |
| 33 | 8 | 12 | 1" | 1 | In-Ladle & In-Stream | 94.8 | 175.1 | 31.55 | 57.21 | 11.24 | 0 | 63.8 | 9.05 | 15.22 | 1.05 |
| 34 | | | 1" | 2 | In-Ladle Only | 90.8 | 109.4 | 21.84 | 47.58 | 30.37 | 0.21 | 89.4 | 9.4 | 13.68 | 0.896 |
| 35 | | | 3" | 3 | In-Ladle & In-Stream | 83 | 115.5 | 29.25 | 48.3 | 21.32 | 1.13 | 119.2 | 9.89 | 17.56 | 1.9 |
| 36 | | | 3" | 4 | In-Ladle Only | 78.3 | 43.2 | 30.83 | 17.65 | 38.47 | 13.04 | 141.5 | 9.6 | 7.98 | 1.34 |

## Analysis of Section Size Effect

The results in Tables 12 and 14 show that some of the properties for the 1 in.Y-blocks have more desirable values than the properties for the 3in.Y-blocks.

Past research on ductile iron has shown that it can exhibit section sensitivity,[22-24] that is, thin section castings with rapid solidification rates will display higher strength and hardness than heavier section castings. The differences are primarily related to (a) coarser cast structures (larger nodules), (b) a larger degree of alloy segregation to the cell boundaries (interdendritic regions) due to longer freezing distances, and (c) higher ferrite contents and coarser pearlite lamellar spacing due to slower cooling rates through the eutectoid transformation region.

With this in mind, the mechanical properties of the 1-in. and 3-in.Y-blocks were compared. The difference in mean hardness between the 1-in. and 3-in.Y-blocks was significant (218 versus 205 HB, respectively). The decrease in average hardness (13 HB units) is relatively small when compared with the full range in hardness (158 to 253 HB) for the variations in alloy content and matrix microstructures in the 1-in.Y-blocks of all nine heats and inoculation conditions. Similarly, the difference in mean yield strength between the 1-in. and 3-in. Y-blocks was relatively small (56 versus 51 ksi, respectively). The decrease in average yield strength (5 ksi) is relatively small when compared with the range in yield strength (45 to 65 ksi) for the variations in alloy content and matrix microstructures in the 1-in.Y-blocks.

When comparing the tensile strength and % elongation in the 1-in. and 3-in. Y-blocks, the reduction in properties was much greater. The reduction in average tensile strength was 13% (97 ksi versus 84 ksi). The reduction in % elongation was 25% (12% versus 9%), and even more substantial. The principal investigators surmise that the reduction in % elongation is directly related to the coarser cast structure and greater alloy segregation in the 3-in. Y-blocks, and the lower UTS values are consistent with a reduction in ductility. The calculation of % strain hardening reflects the same loss in ductility with increasing section size, and this value decreased from 73% to 63%, respectively.

The above analysis suggests that the section size effects are more related to a limitation in ductility with increas-

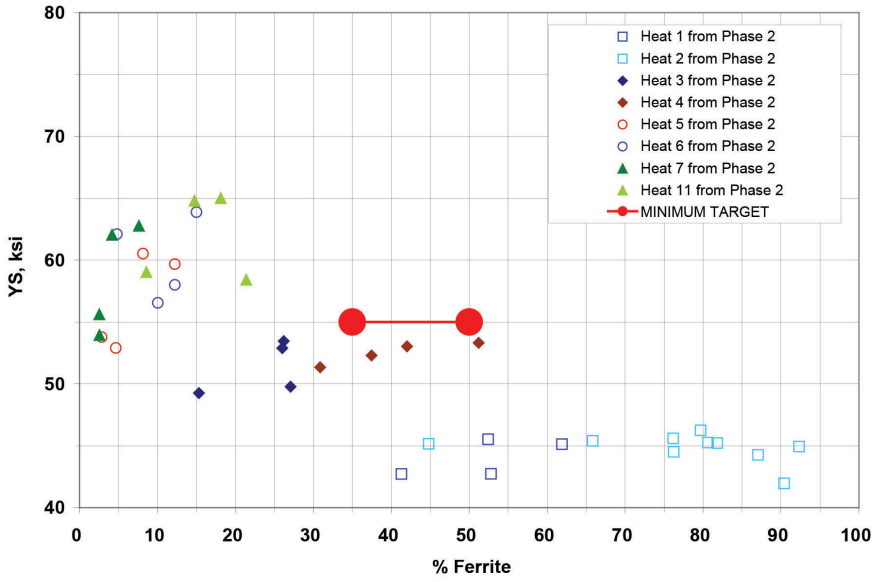


***Figure 22. Yield strength versus ferrite content for Phase 2 DOE results.***

***Table 14. Average Results for the Two DOE Section Sizes***

| Section Size | 1 inch | | | | 3 inch | | | |
|---|---|---|---|---|---|---|---|---|
| | AVERAGES | STANDARD DEVIATION | MINIMUM | MAXIMUM | AVERAGES | STANDARD DEVIATION | MINIMUM | MAXIMUM |
| Brinell Hardness | 218 | 32.3 | 158 | 253 | 205 | 28.8 | 150 | 238 |
| UTS (ksi) | 97 | 17.0 | 67 | 115 | 84 | 9.9 | 64 | 98 |
| YS (ksi) | 56 | 7.6 | 45 | 65 | 51 | 5.8 | 42 | 60 |
| %El at Fracture | 13 | 4.9 | 5 | 24 | 9 | 6.5 | 3 | 22 |
| Reduction of Area (RA), % | 11 | 6.2 | 3 | 26 | 8 | 6.9 | 2 | 25 |
| Elongation (%) | 12 | 5.2 | 4 | 25 | 9 | 6.7 | 3 | 22 |
| Uniform Elongation (%) | 11 | 3.0 | 5 | 17 | 8 | 4.8 | 3 | 16 |
| Strain Hardening (SH), % | 73 | 10.9 | 48 | 88 | 63 | 12.8 | 44 | 85 |
| Toughness, UT (ksi-in/in) | 9 | 2.3 | 3 | 14 | 6 | 3.5 | 2 | 12 |
| Nodularity (%) | 93 | 3.2 | 84 | 97 | 82 | 6.0 | 70 | 92 |
| Nodule Count (mm-2) | 159 | 65.9 | 54 | 265 | 61 | 26.2 | 34 | 119 |
| # of Class 7 (%) | 28 | 12.4 | 14 | 49 | 20 | 5.2 | 14 | 32 |
| # of Class 6 (%) | 53 | 5.8 | 39 | 63 | 32 | 13.2 | 18 | 60 |
| # of Class 5 (%) | 18 | 13.4 | 0 | 40 | 42 | 10.8 | 13 | 53 |
| # of Class 4 (%) | 0 | 1.6 | 0 | 7 | 5 | 3.6 | 0 | 13 |
| Maximum Nodule Size (µm) | 79 | 19.9 | 51 | 124 | 127 | 17.4 | 93 | 161 |
| Graphite Volume Fraction (%) | 9 | 0.8 | 7 | 11 | 9 | 0.6 | 8 | 10 |
| Mean Ferrite Volume Fraction (%) | 34 | 27.7 | 4 | 92 | 30 | 28.2 | 3 | 90 |
| Std. Dev. Ferrite Volume Fraction (%) | 2 | 0.8 | 1 | 4 | 3 | 1.6 | 1 | 6 |

ing section size, as opposed to a reduction in hardness and strength. They also suggest that the effects of section size, as studied in this investigation, are not nearly as pronounced as the effects of alloy content and microstructure.

In order to determine the effect of the section size variation statistically, the principal investigators performed two statistical tests on the average data in Table 16. The first test was a Pearson correlation matrix analysis, and the second test was an unpaired and two-sided Student's t-test.

*Correlation Analyses*

Microsoft Office Excel® was used to conduct Pearson Correlation Analyses as discussed in the Commercial Foundry Data Survey portion of this paper. References 6 and 7 show the r-values obtained for the average mechanical properties, key composition variables, and microstructural parameters as a function of section size shown in Tables 12 and 13. Table 14 shows that the ultimate tensile strength, nodule count, and fine nodule size (% of Class 7 nodules) decrease significantly with increasing section size from 1 in. to 3 in. Furthermore, all mechanical properties (strength, ductility, toughness, and strain hardening) decreased with increasing section size.

### *Student's t-Testing*

Minitab® 15 was used to conduct Student's t-Testing. A two-sample and two-tailed t-test is a hypothesis test for two population means to determine whether they are significantly different. This test essentially determines whether or not there are significant differences between two sets of data.

In this case, the two sets of data in Table 12 were separated, i.e., the collection of average mechanical properties for the 1 in. section size was one dataset and the collection of average mechanical properties for the 3 in. section size was the second dataset. The means and standard deviations were calculated for these two sets of data.

This procedure uses the null hypothesis that the difference between two population means (μ) is equal to a hypothesized (H) value (H0: μ1-μ2 = 0 or μ1 = μ2) and tests it against an alternative hypothesis (H1: μ1≠μ2). One result of the t-test is the value "P". The rejection probability (P), also called alpha (α), was measured for each of the dependent variables versus section size in the t-tests. P ranges from 0 to 1.

The smaller the P-value, the smaller the probability that rejecting the null hypothesis is a mistake. The P-value is calculated from the observed sample and represents the probability of incorrectly rejecting the null hypothesis when it is actually true (Type I error). In other words, it is the probability of obtaining a difference at least as large as the one between the observed value and the hypothesized value through random error alone. After multiplying the P-value by 100 to convert it to a percentage, 100 minus the P% gives the "percent confidence" about stating that the 1 in. section size property differs significantly from the 3 in. section size property. If the test's P-value is less than some chosen level (usually 0.05 or 5%), then H0 should be rejected and H1 accepted.

Figures 23 and 24 show "Box Plots" for the t-testing of two key mechanical properties (hardness and tensile strength) for the two section sizes; similar trends were found in yield strength and elongation. Figure 24 is annotated to show the values that are being plotted inside and outside the boxes, and the captions for all four figures contain the rejection probabilities (P-values) in percentage.

The t-tests showed that all the hardness and tensile properties drop in value as the section size is increased. The decreases in tensile properties are significant with greater than 90% confidence, i.e., P < 10%. The difference in hardness is barely significant, with only 64% confidence, i.e., P ≈ 36%.

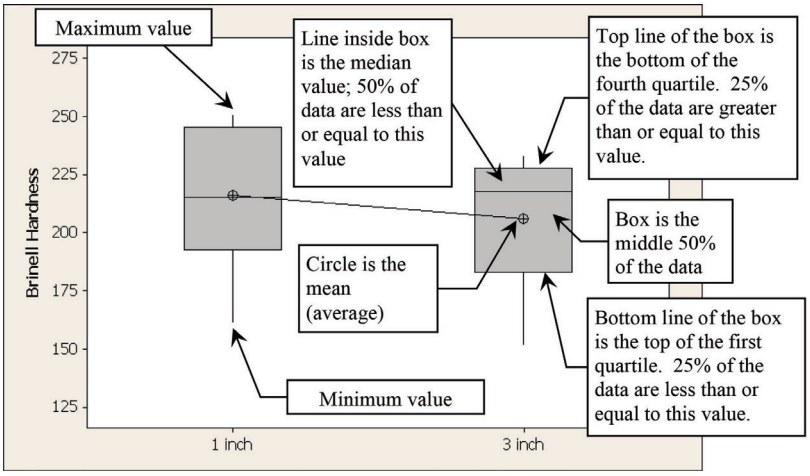


***Figure 23. Student t-test for Brinell hardness as a function of section size with a 35.9% rejection probability (P-value).***

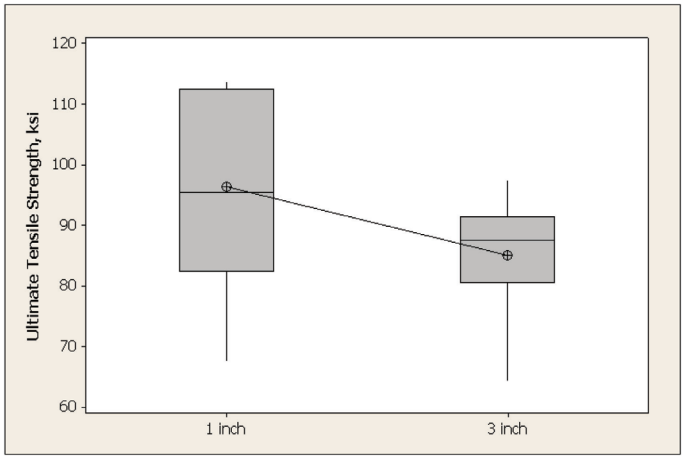


***Figure 24. Student t-test for Ultimate Tensile Strength (UTS) as a function of section size with a 2.8% rejection probability.***

Both the correlation analyses and the student's t-testing showed that section size gives different mechanical property results and the data should be analyzed further by statistical analysis. All trends in composition, microstructure, and mechanical properties were thus analyzed separately for the 1 in. section size and for the 3 in. section size.

## DOE Results

### *Correlation Analyses*

The individual data for the 1 in. section size and for the 3 in. section size were treated separately in Pearson Correlation analyses that were performed in the same manner as previously stated. Again, the authors assigned a value of 1 to "In-Ladle Only" and a value of 10 to In-Ladle & In-Stream to maximize the "chance" of revealing a correlation. The authors performed correlation analysis between all variables for each section size, and also eliminated all composition variables from the analysis to only study the elements that were intentionally varied in the DOE, plus a few major alloying elements. References 6 and 7 contain the mechanical property, composition, and microstructural results for the 1 in. and 3 in. section sizes.

### *Main Effects Analyses*

Minitab was used to conduct "Effects" Analyses from the DOE matrix for both the 1-in. and 3-in. section sizes. Figures 25 to 29 contain "Main Effects Plots" for some of the key dependent mechanical property variables (responses) measured in this study for the 1-in. section size versus the independent DOE variables (stimuli) or "factors." Figure 25 is annotated to help explain the various characteristics of a main effect plot. Other Main Effect Plots are contained in References 6 and 7. Also, the Main Effect Plots obtained for the 3-in. section size were similar to those obtained for the 1 in. section size.

The key mechanical property response variables are as follows: Brinell hardness, ultimate tensile strength, yield strength, elongation, reduction of area, toughness and strain hardening. A main effects plot is a plot of the means of the key mechanical property variables at each level of a factor. In this study, there were four factors (independent variables or stimuli). The four factors were inoculation method, silicon content, manganese content and copper content, each varied at two levels, for each of the section sizes (1 in. and 3 in.).

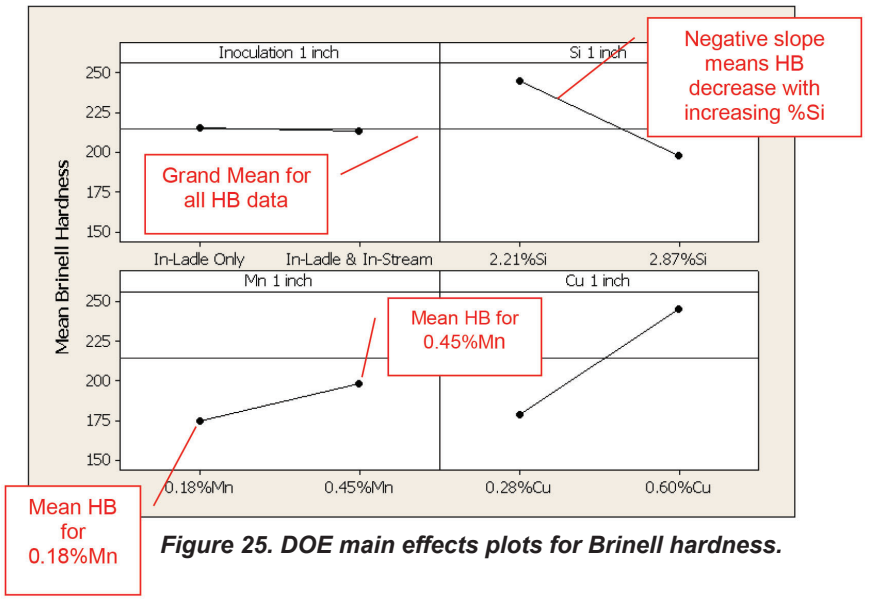


*Figure 25. DOE main effects plots for Brinell hardness.*

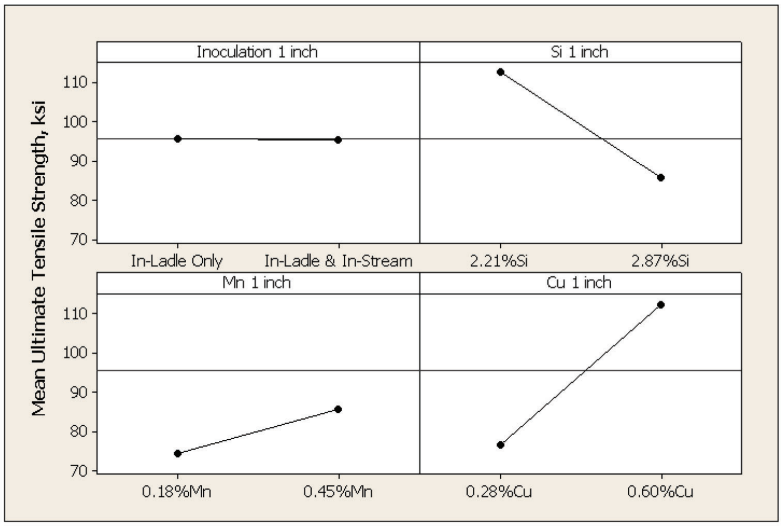


*Figure 26. DOE main effects plots for ultimate tensile strength.*

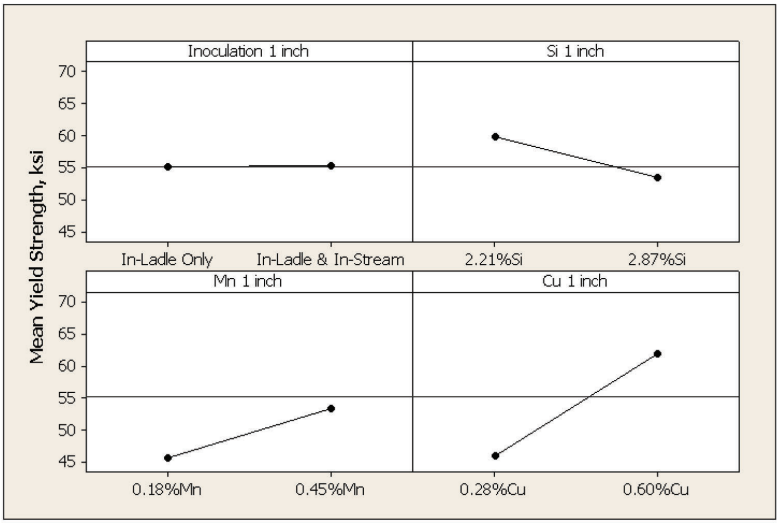


*Figure 27. DOE main effects plots for yield strength.*

The main effects plots utilized the raw response data, and plotted points for the means at each level of the factor and connected them with a line. The horizontal line in each plot is a reference line at the grand mean of the response data. The program also draws a separate plot for each factor-response combination. A main effect occurs when the mean response changes across the levels of a factor, and you can use main effects plots to compare the relative strength of the effects across factors.

### *Factorial Fit Analyses*

Although the main effects plots of the analyses show the "magnitude" of the effects for the various variable combinations, these plots contain no statistical significance information. Minitab was used to conduct factorial fit analyses for the Main and Interaction Effects for both the 1 in. and 3 in. section sizes. The rejection probabilities results from the factorial fit analyses are contained in References 6 and 7.

### *Pareto Charts of the Effects*

Software was used to conduct Pareto analyses for the Main and Interaction Effects. Figure 30 contains a "Pareto Plot" for a selected key dependent mechanical property variable (response) measured in this study versus the independent DOE variables (stimuli) or "factors" for the 1 in. section size. Similar Pareto Plots were obtained for the other variables in the 1 in. and 3 in. section sizes and these are contained in References 6 and 7. Figure 30 is annotated to help explain the various characteristics of a Pareto chart.

A Pareto chart of the effects is used to determine the magnitude and the importance of an effect. The chart displays the Student's t-value of each main or interaction effect. Minitab draws a reference line on the chart. Any effect that extends past this reference line is potentially important. Minitab uses Lenth's method[26] to draw the line. The reference line corresponds to a rejection probability of P or $\alpha$ equal to 0.05 or 5%.

### *Summary of the Statistical Analyses*

Recall that the key mechanical property response variables are as follows: Brinell hardness, ultimate tensile strength, yield strength, elongation, reduction of area, toughness and strain hardening, and that there were four factors (independent variables or stimuli) as follows: Inoculation type, Silicon content, Manganese content and Copper content, each varied at two levels, for each of the section sizes (1 in. and 3 in).

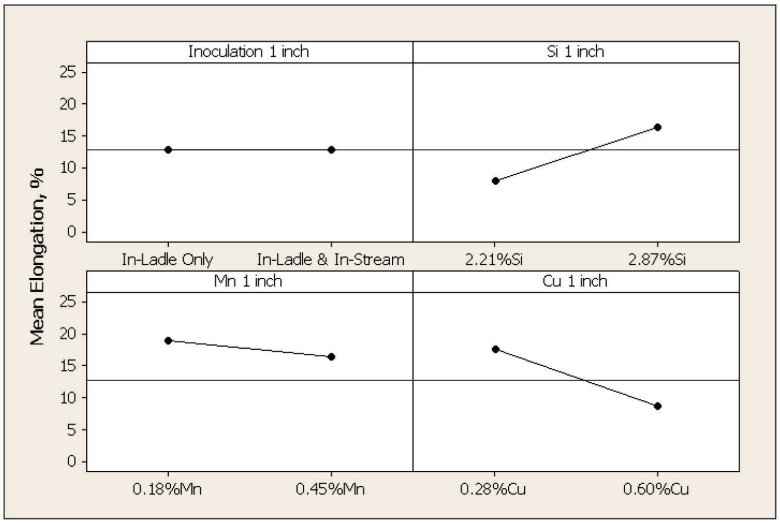


*Figure 28. DOE main effects plots for elongation.*

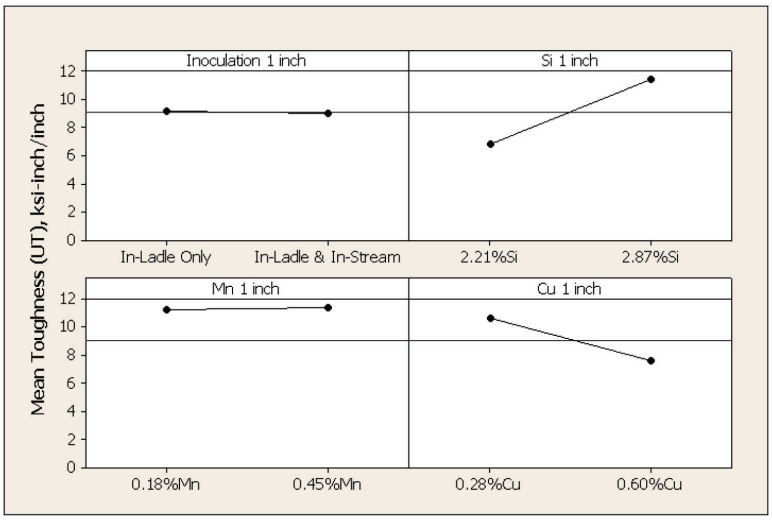


*Figure 29. DOE main effects plots for toughness.*

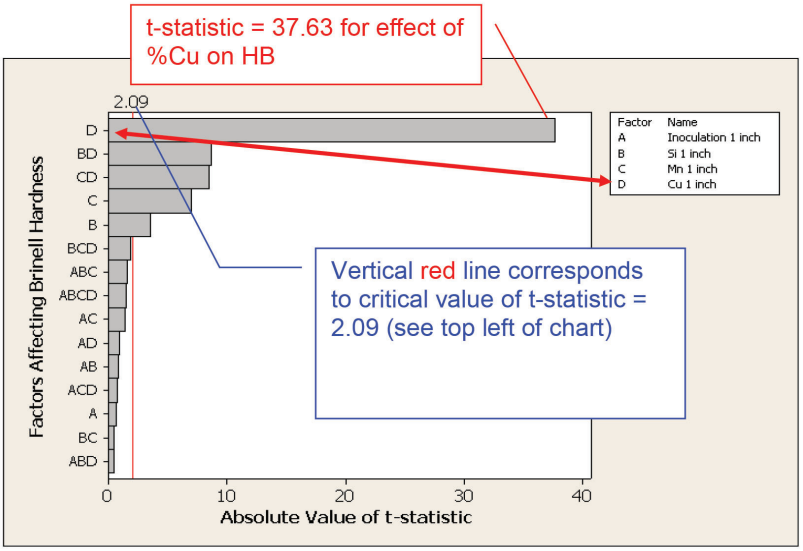


***Figure 30. DOE Pareto Plot for the effects on hardness.***

For the 1 in. section size, Table 15 shows the key mechanical properties as a function of the three statistical parameters and the four DOE variables. Similar summary results were obtained for the 3 in. section size but are not shown in this paper. An "X" signifies that the stimulus had a significant effect on the response, and a plus (+) or minus (-) sign indicates the direction of the effect.

For both section sizes, the following trends were noted:

- Increasing Cu and/or Mn contents increased strength and hardness
- Increasing Cu and/or Mn contents decreased ductility and toughness (UT)
- Increasing Si content generally decreased strength and increased ductility
- In all (but one minor case), inoculation had no effect on mechanical properties

Somewhat different trends were noted for the two section sizes as follows:

- Varying Mn was more effective than Cu in affecting the properties in the 3 in. section size
- Varying Si was less effective in the 3 in. section size versus the 1 in. section size
- Both strength and ductility were higher in the 1 in. versus the 3 in. section size (also see Table 14)

Table 14 demonstrates that all the mechanical properties (both strength and ductility) were higher in the 1 in. section size versus the 3 in. section size. Since the properties were so much lower in the 3 in. section size, the alloying effects were less potent in the 3 in. section size. This aspect is consistent with earlier section sensitivity work.[23-25]

For the most part, the addition of in-stream inoculation did not significantly increase any silicon content, microstructural, or mechanical property as compared to utilizing ladle inoculation by itself. Late stream inoculation is a proven method to improve nodularity and nodule count. The absence of such improvements in this study could mean that the ladle inoculation technique and pouring sequence had already maximized the inoculation effect, or it could mean that the technique selected for this study was neither effective nor ineffective. In any event, the study results should not detract from the known fact that late stream inoculation is an effective means of maximizing nodularity and nodule count.

As discussed above, the three alloying variables all contributed to the observed variations in mechanical properties, although changing the copper content had the most potent main effect on mechanical properties. A "main" effect means that there is a relationship between any mechanical property (dependent variable) and a single elemental content (independent) variable. Table 15 and the Pareto plot in Figure 30 show that a few two-way and three-way interactive effects in the composition variables had some selected effect, but there were no consistently effective interaction alloy terms. From a practical standpoint, the copper addition effects of increasing strength and decreasing elongation are consistent with existing theory and practice.

It should be noted that the authors performed an evaluation of the various microstructural parameters (e.g., nodule count) as a function of changes in the DOE variables. However, the trends in the data were not visually apparent in simple X-Y plots of the data and the trends were not statistically significant. Therefore, no such results are presented in this paper.

The Pearson Correlation Analysis and various statistical routines conducted in the DOE showed that excellent variables and variable levels were selected for the DOE. Major effects and their magnitudes were clearly identified, or they were absent, so that strong conclusions could be drawn.

## Alloying Trends

Examination of the data in Figures 21 and 22, as well as in the DOE Main Effects plots in Figures 25 to 29 from this study, show the following effects of the alloying elements:

- Copper is more effective than manganese in increasing pearlite content, i.e., there is a more negative correlation coefficient in the relationship between copper and ferrite contents versus manganese and ferrite contents.

***Table 15. Summary of all DOE Statistical Test Results for 1" Section Size***

| **Inoculation** | **HB** | **UTS** | **YS** | **El** | **RA** | **$U_T$** | **SH** |
|---|---|---|---|---|---|---|---|
| Main Effect Plot | | | | | | | |
| Rejection Probability Table | | | | | | X | |
| Pareto Chart | | | | | | | |
| | | | | | | | |
| **Si** | **HB** | **UTS** | **YS** | **El** | **RA** | **$U_T$** | **SH** |
| Main Effect Plot | - | - | - | + | + | + | - |
| Rejection Probability Table | X | X | X | X | X | X | X |
| Pareto Chart | | X | X | X | X | | X |
| | | | | | | | |
| **Mn** | **HB** | **UTS** | **YS** | **El** | **RA** | **$U_T$** | **SH** |
| Main Effect Plot | + | + | + | | | | |
| Rejection Probability Table | X | X | X | | | | |
| Pareto Chart | X | X | X | X | | | |
| | | | | | | | |
| **Cu** | **HB** | **UTS** | **YS** | **El** | **RA** | **$U_T$** | **SH** |
| Main Effect Plot | + | + | + | - | - | - | + |
| Rejection Probability Table | X | X | X | X | X | X | X |
| Pareto Chart | X | X | X | X | X | X | X |
| | | | | | | | |

- Copper is also more effective than manganese in increasing strength. Figure 33 shows that the high-Cu experimental casting alloys #5 and #6 have higher yield strength and elongation combinations than the trend line from the Commercial Foundry Data Survey. In contrast, the high-Mn experimental casting alloys #3 and #4 have lower yield strength and elongation combinations than the trend line from the Commercial Foundry Data Survey.

## Selection of a Heat for Validation

The principal investigators selected one heat composition to confirm the results from the foundry that cast the DOE heats. It was important that one of the eight DOE heat compositions was selected to ensure that an uncontrolled variable did not enter into the study. However, a secondary hope was that the verification heat might have the best opportunity to achieve the simultaneously high strength and ductility targets. Foundry E from the Commercial Foundry Data Survey was chosen for casting the verification heat.

Based on the results of this study, particularly in Table 10 and Figure 21, the principal investigators chose to validate by casting 1-in.Y-blocks of Heat #6. The three main elements in the study were Si, Mn, and Cu. Nominal aim for the verification heat with these three elements was as follows: 2.6% Si, 0.3% Mn, and 0.6% Cu. Other details of the casting operation are contained in Reference 6.

The verification results are shown in Table 16. The results of the new repeat heat essentially duplicated those of DOE Heat #6 with equivalent composition, microstructure, strength and ductility.

***Table 16. Results from Verification Heat "V" vs. Heat 6 (in red) from DOE Study***

| **Overall Sample #** | 60 | 61 | | 90 | 91 | 92 | |
|---|---|---|---|---|---|---|---|
| **Cast Section Size** | 1" Y block | | | | | | |
| **Heat #** | 6 | 6 | | V | V | V | **V** |
| **Replicate** | A | B | **Ave** | A | B | C | **Ave.** |
| **Mold** | 2 | 2 | | 1 | | | |
| **Inoculation** | In-Ladle | | | | | | |
| **Position** | Bottom | Bottom | | Bottom | Bottom | Bottom | |
| **Brinell Hardness** | 246 | 246 | **246** | 239 | 232 | 231 | **234** |
| **UTS (ksi)** | 112.5 | 112.9 | **112.7** | 110.8 | 111.5 | 111.4 | **111.2** |
| **YS (ksi)** | 63.87 | 64.3 | **64.1** | 62.6 | 63.3 | 63.0 | **63.0** |
| **%El(at Fracture by Extensometer)** | 10.9 | 10.1 | **10.5** | 8.7 | 10.1 | 9.2 | **9.4** |
| **%RA** | 8.0 | 8.3 | **8.1** | 6.3 | 7.7 | 7.5 | **7.2** |
| **% Elong.** | 10.8 | 10.0 | **10.4** | 7.4 | 9.8 | 8.6 | **8.6** |
| **Uniform Elongation (%)** | 10.7 | 9.8 | **10.2** | 8.7 | 9.8 | 9.2 | **9.2** |
| **(UTS-YS)/YS (%)** | 76.1 | 75.5 | **75.8** | 77.1 | 76.2 | 76.8 | **76.7** |
| **Toughness, UT (ksi-in/in)** | 9.5 | 8.8 | **9.2** | 6.4 | 8.6 | 7.5 | **7.5** |
| **Nodularity (%)** | 96.5 | | **96.5** | 95.7 | 95.9 | | **95.8** |
| **Nodule Count ($mm^{-2}$)** | 168 | | **168** | 141.5 | 133.4 | | **137.5** |
| **# of Class 7 (%)** | 30.4 | | **30.4** | 26.1 | 25.5 | | **25.8** |
| **# of Class 6 (%)** | 58.8 | | **58.8** | 56.7 | 56.2 | | **56.5** |
| **# of Class 5 (%)** | 10.8 | | **10.8** | 17.1 | 18.2 | | **17.6** |
| **# of Class 4 (%)** | 0 | | **0** | 0.1 | 0.0 | | **0.1** |
| **Maximum Nodule Size (µm)** | 70.6 | | **70.6** | 98.9 | 83.2 | | **91.1** |
| **Graphite Volume Fraction (%)** | 8.9 | | **8.9** | 9.0 | 8.9 | | **9.0** |
| **Mean Ferrite Volume Fraction (%)** | 15.0 | | **15.0** | 13.3 | 14.9 | | **14.1** |
| **Std Dev Ferrite Volume Fraction (%)** | 1.31 | | **1.31** | 1.0 | 1.2 | | **1.1** |
| **C** | 3.49 | | **3.49** | 3.71 | 3.68 | 3.69 | **3.69** |
| **S** | <0.005 | | **<0.005** | 0.009 | 0.008 | 0.008 | **0.008** |
| **P** | 0.029 | | **0.029** | 0.012 | 0.014 | 0.013 | **0.013** |
| **Si** | 2.71 | | **2.71** | 2.62 | 2.61 | 2.62 | **2.62** |
| **Mn** | 0.28 | | **0.28** | 0.34 | 0.35 | 0.34 | **0.34** |
| **Cr** | 0.04 | | **0.04** | 0.06 | 0.06 | 0.07 | **0.06** |
| **Ni** | 0.02 | | **0.02** | 0.02 | 0.02 | 0.06 | **0.03** |
| **Mo** | <0.01 | | **<0.01** | 0.01 | 0.01 | 0.01 | **0.01** |
| **V** | 0.006 | | **0.006** | 0.018 | 0.019 | 0.021 | **0.019** |
| **Al** | 0.009 | | **0.009** | 0.012 | 0.012 | 0.013 | **0.012** |
| **Cu** | 0.57 | | **0.57** | 0.59 | 0.58 | 0.58 | **0.58** |
| **Mg** | 0.04 | | **0.04** | 0.05 | 0.054 | 0.053 | **0.052** |
| **Ti** | 0.01 | | **0.01** | 0.010 | 0.012 | 0.012 | **0.011** |
| **Sb** | <0.005 | | **<0.005** | <0.005 | <0.005 | <0.005 | **<0.005** |
| **Ce** | 0.01 | | **0.01** | 0.010 | 0.011 | 0.008 | **0.010** |
| **Sn** | <0.005 | | **<0.005** | <0.005 | <0.005 | <0.006 | **<0.006** |
| **Carbon Equivalent (CE)** | 4.40 | | **4.40** | 4.59 | 4.55 | 4.57 | **4.57** |

## Heat Treatment Effect

A few unconventional heat treatments were employed on selected alloys from the experimental castings research portion of this study in an attempt to produce fine-grained microstructures, which might exhibit improved combinations of mechanical properties. The inspiration for this investigation was provided by an earlier study[27] wherein heat treatment in the intercritical region produced a microstructure consisting of fine-grained acicular austenite in proeutectoid ferrite. When quenched from the intercritical temperature, the acicular austenite transformed to martensite, and the as-quenched microstructure displayed a significant amount of grain refinement over the as-cast structure.

It was also anticipated that air-cooling from the intercritical temperature will produce a similar fine-grained structure consisting of acicular pearlite in ferrite. Indeed, one of the sponsors submitted a commercial casting with such a microstructure, as shown in Figures 31 and 32. This commercial casting displayed mechanical properties of 225 HB, 66 ksi YS, 105 ksi UTS, and 10% elongation.

In typical cast iron alloys, which contain substantial amounts of silicon, the eutectoid transformation region contains a three-phase field where austenite, ferrite and graphite co-exist. The three-phase region is shown in Figure 33. In conventional ductile iron chemistries, the lower critical and upper critical temperatures are separated by anywhere from 67 to 89˚C (120 to 160˚F). Upon heating between the lower and upper critical temperatures, the volume fraction of austenite increases with temperature. Upon exceeding the upper critical, the remaining ferrite disappears and a 100% austenite structure develops.

While heating in the intercritical region, the metallic matrix is partially austenitized by recarburization of the ferritic-pearlitic matrix. It is hypothesized that recarburization of the matrix occurs by the dissolution of graphite and the diffusion of carbon along the ferrite grain boundaries that intersect the graphite nodule. Subsequently, carbon migrates from the grain boundaries into the ferrite matrix along intercrystalline planes to produce lenticular grains of austenite within the ferrite grain. The austenite grains nucleate and grow from the ferrite grain boundaries outward into each ferrite grain, as depicted in Figure 34. Once equilibrium is achieved, the resultant microstructure consists of numerous acicular austenite grains surrounded by the parent ferrite grains which, at the intercritical temperature, are stable and in equilibrium with the austenite phase. At higher intercritical temperatures the austenite fraction is high and the acicular structure is well-developed.

When quenched in oil from the intercritical temperature, the austenite transforms to martensite, producing a relatively high-strength material with modest ductility. On tempering, the martensite becomes tempered and ductility improves.

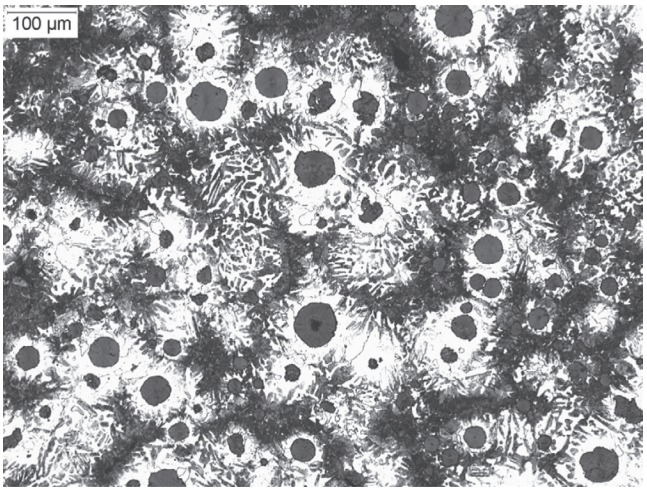


***Figure 31. Optical micrograph of commercial casting that was probably intercritically heat treated. 2% nital, Original Magnification (OM) = 50X.***

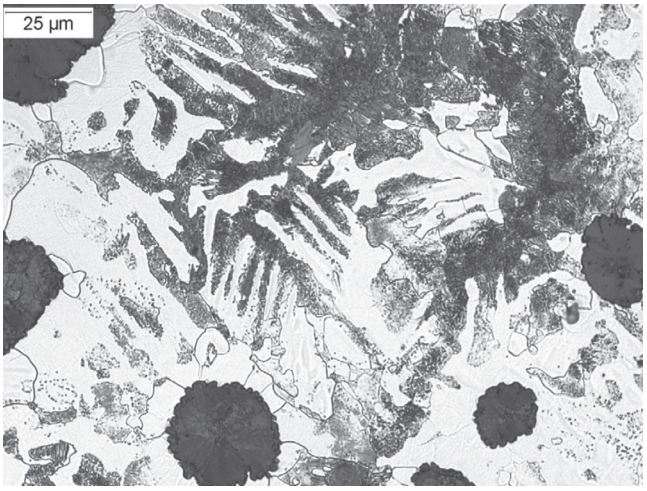


***Figure 32. Optical micrograph of commercial casting that was probably intercritically heat treated. 2% nital, Original Magnification (OM) = 500X***

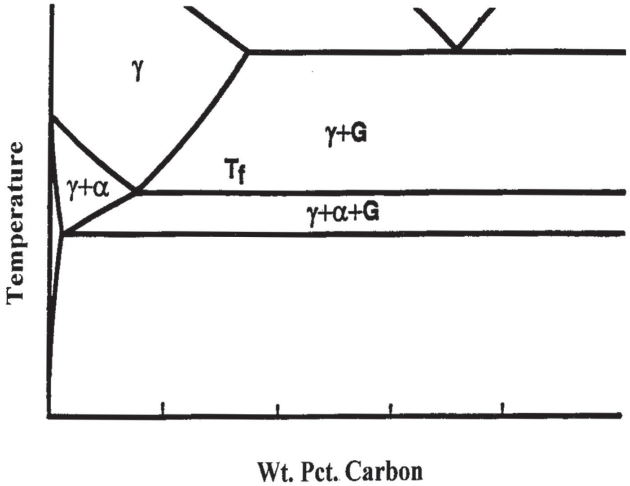


***Figure 33. Schematic of a portion of a Fe-C-Si phase diagram illustrating the three phase region where austenite, ferrite and graphite coexist.***

Depending upon the tempering temperature, the extent of martensite tempering varies and the balance between strength and ductility changes.

Alternatively, with air-cooling, the fine-grained austenite that formed at the intercritical temperature will transform to pearlite colonies with an acicular morphology, resulting in a fine-grained ferrite-pearlite structure.

***Note**: A grain signifies one crystallographic orientation. Therefore, a "pearlite grain" is never a proper usage since there are two sets of crystallographic orientations in pearlite, i.e., one crystallographic orientation in the ferrite phase and the other orientation in the cementite phase. The acicular terminology is used herein to describe a single set of crystallographic orientations in the cooperative growth of ferrite and cementite, which forms a single "microstructural unit" of pearlite. In one textbook,[27] a pearlite nodule combines with one or more other pearlite nodules to form a colony, i.e., a pearlite nodule is a subset of a colony. In another literature source,[28] which reviews multiple references of pearlite formation, a pearlite colony is a subset of a pearlite nodule. In any case, the smaller unit that is equivalent to a grain of proeutectoid ferrite is under discussion herein.*

The proportion of ferrite and pearlite is somewhat dependent on the cooling rate. It is anticipated that with slower cooling some austenite will decompose to ferrite and graphite prior to reaching the pearlite nose. Consequently, the fine-grained structure developed during intercritical heating may become somewhat degraded on air-cooling. It is not possible to inhibit austenite from reverting to ferrite, except by rapid quenching in oil or by forced-air cooling. (Alloying with copper and tin may also cause the austenite to be more stable, but here we are studying heat treatment alone.)

The proportion of ferrite and acicular austenite that develops is a function of the intercritical temperature and chemical composition. As demonstrated earlier,[27] chemical composition has a significant effect on the upper and lower critical temperatures in ductile iron. The optimum amount of austenite (and the proper intercritical temperature) required to achieve the best mechanical properties must be determined by experiment.

For this investigation, Conditions #20, #44 and #52 (see Table 11) were selected for the heat treatment study. These three samples represented equivalent section size (1 in.) and inoculation (In-Ladle & In-Stream) of three different heats, i.e., Heats 2, 4, and 5 in Table 15, respectively. These three heats represent alloys having as-cast microstructures consisting of predominantly ferrite, an equal mixture of ferrite and pearlite, and predominantly pearlite, respectively.

Three heat treatment trials were conducted. For the sake of brevity, Reference 21 contains the mechanical properties and microstructures for the first two trials although the descriptions are included in this paper.

### *First Heat Treatment Trial*

The first heat treatment study was conducted with 5/8 in. by 1 in. by 1 in. samples with variations in heat treatment temperature and cooling rate. All the conditions involved heating for one hour at the intercritical heat treatment temperature, followed by still-air cooling, forced-air cooling or oil-quenching, where quenching was performed. When tempering was performed, the samples were tempered for two hours at the tempering temperature.

The same intercritical temperatures were chosen between the upper and lower critical temperatures, which were calculated from published work.[27] The upper and lower critical temperatures varied slightly for the three Heats 2, 4 and 5.

The microstructures of the heat treated samples were generally refined as compared to the as-cast samples, which is consistent with the significant increase in hardness of the small samples versus the as-cast condition. Upon examination of the microstructures, the results showed that the best starting microstructure prior to heat treatment is a fully ferritic material. Furthermore, the microstructures of the heat treated samples were very similar to those that the investigators examined at the outset of this study for the commercial castings that were shown in Figures 31 and 32.

### *Second Heat Treatment Trial*

Subsequently, in a second series of heat treatment experiments, Y-block legs were heat-treated to selected heat treatment cycles quite similar to those of the first heat-treatment trial. The tensile properties and hardness of these heat-treated Y-block legs were determined.

While the hardness increased with heat treatment of the small samples, the trend was less pronounced when full tensile sections were heat treated. Although the heat treatments were designed to produce microstructural manipulations to search for trends, only the heat treatment of sample 4 showed some promise versus its as-cast condition, wherein the strengths remained constant but the reduction in area increased.

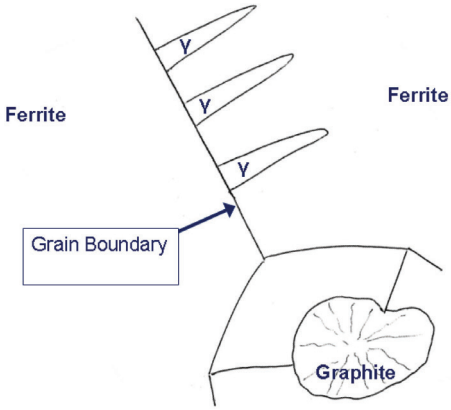


***Figure 34. Hypothetical illustration depicting the nucleation and growth of lenticular austenite grains on ferrite grain boundaries during the recarburization of the metallic matrix on heating above the lower critical temperature.***

Although the second heat treatment trial samples showed general structural refinement as compared to the as-cast samples, section size during heat treatment strongly affected the hardness and microstructure balance. Much less structural refinement was observed in the heat treated tensile blanks as compared to the small samples.

### *Third and Final Heat Treatment Trial*

The previous experiments with intercritical (IC) heat treatment indicated that at the IC temperature, the microstructure consists of "acicular" austenite grains in ferrite. The acicular austenite grains had limited stability on cooling from the intercritical temperature to below the lower critical temperature ($A_1$). With small test samples, the desired microstructure was achieved. However, with air-cooling of the 1 x 1 x 6 in. Y-block leg, the austenite partially decomposed to ferrite and graphite, the hardness and tensile properties decreased, and the ferrite content increased.

For the third and final heat treatment experiments, the heat treatment temperatures and cooling rates were adjusted. Only Y-block legs from Heats 2 and 4 were chosen for heat treatment. The following three different approaches were investigated:

1. Forced-air cooling of the Y-block leg should help to inhibit decomposition of the austenite to ferrite before reaching the pearlite nose.
2. With still air-cooling, it was anticipated that excess austenite decomposition will occur. Therefore, still-air cooling from a higher intercritical temperature was attempted. In this manner, the final pearlite content will remain relatively high.
3. Oil-quenching was repeated and two lower tempering temperatures were applied to try and develop a fine-grained acicular martensite in ferrite, having a higher hardness and strength.

The following experiments were performed:
Experiment #1: (Y-block legs from Heats #2 and #4)

- Heat treat from similar intercritical temperatures (see Table 17) as the second heat treatment trial and apply forced-air cooling
- Conduct hardness, tensile testing and metallography (including determination of % ferrite)

Experiment #2: (Y-block legs from Heats #2 and #4)

- Heat treat from a higher intercritical temperature (see Table 17) versus the second heat treatment trial and apply still-air cooling.
- Conduct hardness, tensile testing and metallography (including determination of % ferrite)

Experiment #3: (Y-block legs from Heats #2 and #4)

- Heat treat from a similar intercritical temperature (see Table 17) as the second heat treatment trial and oil quench
- Then, temper for 2 hours at two different temperatures (between 500F and 900F) to vary the hardness and mechanical properties
- Conduct hardness, tensile testing and metallography (including determination of % ferrite)

Tables 17 and 18 show the results. The most promising conditions to meet the >55 ksi YS, >80 ksi UTS, and >12% Elongation goals are shown in red in Table 18.

All of the third trial heat treatment data are also plotted in Figure 35 for comparison with the as-cast properties of the materials from the commercial foundry data survey and the DOE study, as well as the yield strength and elongation specifications for the standard grades 40-18, 45-12, 55-06, 70-03, and 90-02. Figure 35 shows that the quench and temper heat treatments exhibit much higher strength at equivalent ductility than the normalized heat treatments, the Phase 1 trend line, and the specifications for the standard grades.

Several conditions exceeded the goals of this study. Although the 12% elongation minimum was not quite achieved, the Q&T produced higher strengths at equivalent ductilities for many of the lower strength grades in the as-cast ASTM A536 grades. The most promising results were obtained by

***Table 17. Results of Third Heat Treatment Trials***

| Sample ID | Heat No. | Starting Microstructure | Intercritical Heat Treatment Temperature & Subsequent Condition | Brinell Hardness | Ferrite Content |
|---|---|---|---|---|---|
| #20 | 2 | 92%F-8%P | As-Cast (No Heat Treatment) | ***158*** | ***92*** |
| 2A-FAC | | | 1525F + Forced Air Cool | 183 | 73 |
| 2B-AC | | | 1545F + Air Cool | 232 | 38 |
| 2C-Q&T-L | | | 1525F Q&T at 800F | 300 | 27 |
| 2D-Q&T-H | | | 1525F Q&T at 925F | 283 | 45 |
| | | | | | |
| #44 | 4 | 51%F-49%P | As-Cast (No Heat Treatment) | ***196*** | ***51*** |
| 4A-FAC | | | 1525F + Forced Air Cool | 195 | 67 |
| 4B-AC | | | 1545F + Air Cool | 245 | 39 |
| 4C-Q&T-L | | | 1525F Q&T at 800F | 323 | 22 |
| 4D-Q&T-H | | | 1525F Q&T at 925F | 296 | 55 |

***Table 18. Mechanical Properties Resulting from Third Heat Treatment Trial***

| Sample ID | Heat | Condition | Hardness HBW3000 | YS, ksi | UTS, ksi | %El | %RA | Ferrite % |
|---|---|---|---|---|---|---|---|---|
| 1 | 2 | 2A-FAC | 183 | 52.5 | 84.0 | 11.0 | 15 | 73 |
| 2 | 2 | 2B-AC | 232 | 61.0 | 103 | 11.6 | 9.0 | 38 |
| 3 | 2 | 2C-Q&T-L | 300 | 79.5 | 133 | 7.0 | 6.0 | 27 |
| 4 | 2 | 2D-Q&T-H | 283 | 78.5 | 126 | 8.0 | 7.0 | 45 |
| 5 | 4 | 4A-FAC | 195 | 57.5 | 90.5 | 9.6 | 15 | 67 |
| **6** | **4** | **4B-AC** | **245** | **67.0** | **110** | **9.0** | **8.0** | **39** |
| 7 | 4 | 4C-Q&T-L | 323 | 89.5 | 140 | 3.4 | 3.5 | 22 |
| **8** | **4** | **4D-Q&T-H** | **296** | **85.0** | **132** | **7.6** | **5.5** | **35** |

quenching and tempering the heat with a starting 50:50 ferrite pearlite ratio. For the still-air cooled and forced-air cooled samples, the ferrite content decreased significantly over those of heat treatment Trial 2, and the combinations of strength and ductility were promising.

Figures 36 to 39 show typical micrographs for the conditions colored in red in Table 18. Selected phases are labeled in Figures 37 and 39. These heat treated samples exhibit significant structural refinement as compared to the corresponding micrograph for the as-cast condition from Heat #4, which is shown in Figure 40.

It is interesting to note that, when plotted against ferrite content, the yield strengths of the heat-treated test bars are

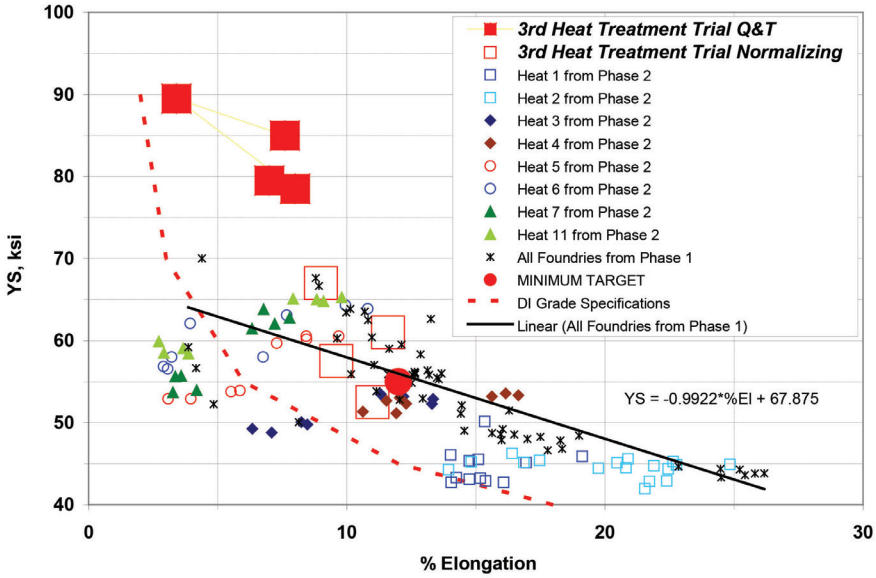


***Figure 35. Results of the Third Heat Treatment Trials with the as-cast data from Phase 1 and Phase 2.***

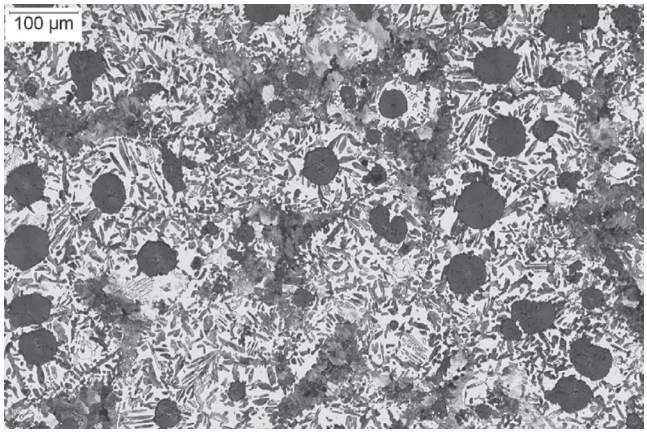


***Figure 36. Third Heat Treatment Trial, Sample ID 6, Heat 4, Condition 4B-AC (1545 F Intercritical plus Air Cool). 2% Nital, 100X.***

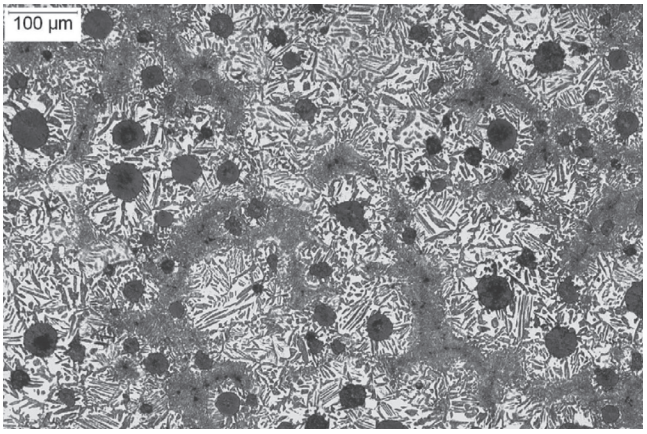


***Figure 38. Third Heat Treatment Trial, Sample ID 8, Heat 4, Condition 4C-Q&T-H (1525 F Intercritical plus Q&T at 925F). 2% Nital, 100X.***

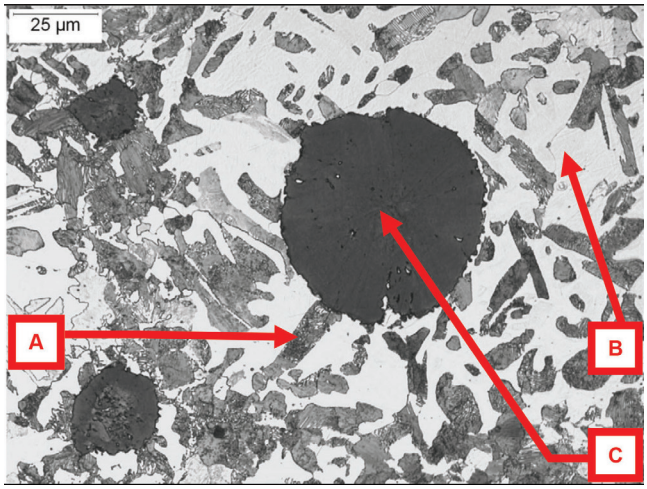


***Figure 37. Third Heat Treatment Trial, Sample ID 6, Heat 4, Condition 4B-AC (1545 F Intercritical plus Air Cool). Constituent A is an acicular pearlite colony, constituent B is ferrite, and constituent C is a graphite nodule. 2% Nital, 500X.***

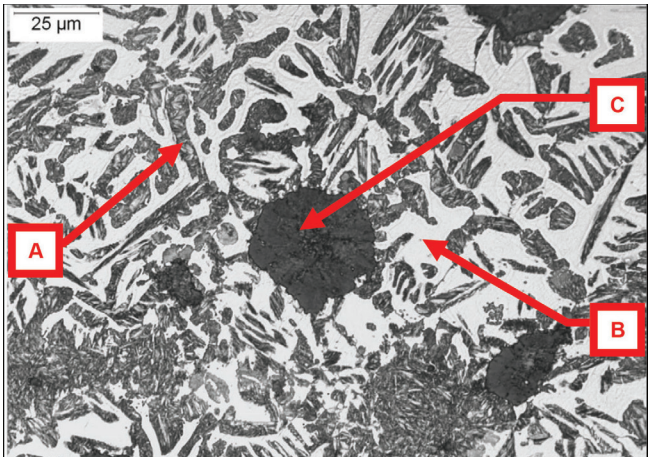


***Figure 39. Third Heat Treatment Trial, Sample ID 8, Heat 4, Condition 4C-Q&T-H (1525 F Intercritical plus Q&T at 925F). Constituent A is an acicular martensite grain, constituent B is ferrite, and constituent C is a graphite nodule. 2% Nital, 500X***

generally higher than those of the as-cast materials of this study, see Figure 41. The elevated ferrite content in the heat-treated alloys is expected to provide improved machinability when compared to as-cast materials produced to the same strength level.

It should be noted that intercritical heat treatments have also been studied by others. There is a relatively common grade of austempered ductile iron that consists of austempering from an intercritical temperature. An alternate form of intercritical heat treatment has also been described by Franco Zanardi.[30] The properties achieved by Mr. Zanardi overlap those of this study. However, Mr. Zanardi's heat treatment parameters were not well documented, and are unavailable for discussion in this paper.

Figures 42 and 43 show that the results of this heat treatment study point to partial success towards fulfilling the original goals of this study. Figure 42 shows that many of the heat treated castings have greater strength and greater ductility than as-cast materials. Figure 43 shows that the better properties were obtained in several of the R&D castings versus commercial castings and standard ductile iron specifications.

## Conclusions

Based on the results of the commercial foundry data survey, the following conclusions were reached:

1. The traditional relationship between ferrite content and ductile iron mechanical properties was confirmed and quantified. As ferrite content increases, strength in the form of ultimate strength and yield strength decrease, and elongation increases.
2. The literature predicts that decreasing grain size strongly increases yield strength but can only be accomplished with post solidification heat treatment. The results of this study confirmed that trend, although finer grain size was measured adjacent to graphite nodules.
3. The alloying elements copper, manganese, copper + manganese and silicon strongly influence the occurrence of ferrite and, just as importantly, can be numerically correlated to the resulting mechanical properties.
4. An "ideal" range for copper, manganese, copper + manganese, and silicon can be related to achieving yield strengths in excess of 55 ksi combined with elongations that exceed 12%.
5. Manual and automated image analysis measurements of ferrite content show excellent agreement and ferrite grains almost always touch graphite nodules.
6. The contiguous nature of ferrite colonies appears to be related to mechanical properties. An increase in ferrite colony continuity reduced the strength and ductility of samples with nominally the same ferrite content and graphite parameters, and a similar strength reduction with the dendrite alignment direction was reported in the literature.

Based on the results of this DOE investigation, the following conclusions were reached:

1. Both correlation analysis and the Student's t-testing showed that section size gave different mechanical property results. Some of the properties obtained

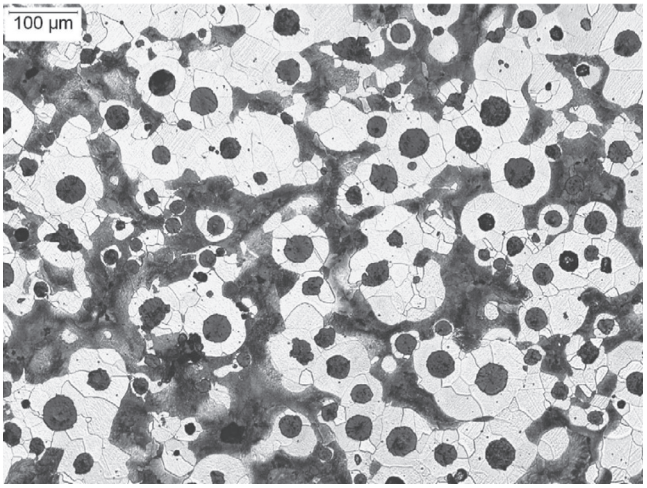


***Figure 40. Optical Micrograph of ferritic-pearlitic as-cast sample #44 from Heat #4. 2% nital, Original Magnification (OM) = 100X***

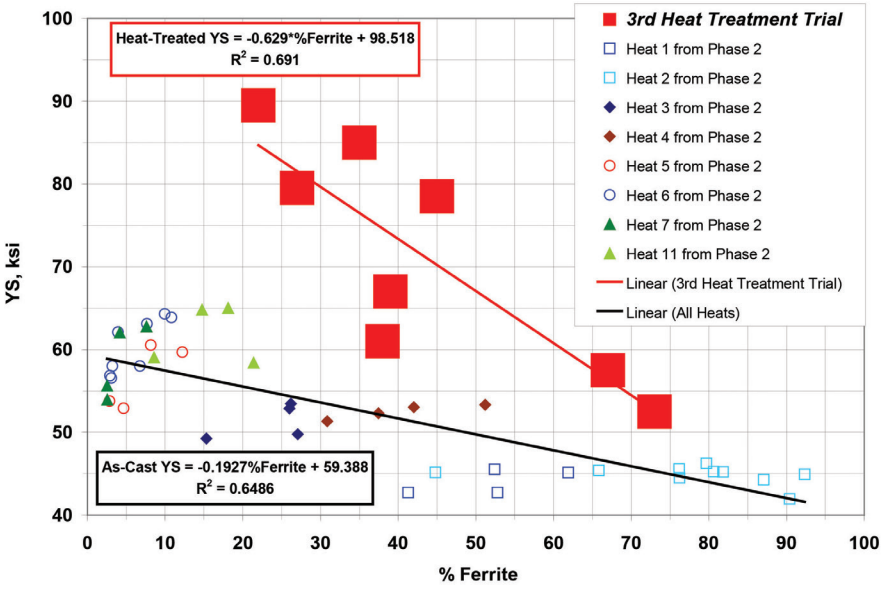


***Figure 41. Results of the Third Heat Treatment Trials with the as-cast data from Phase 2. Note that the heat treated samples (red) have higher ferrite contents than the as-cast samples.***

for the 1-in.Y-blocks were better than the properties for the 3 in.Y-blocks. The section size effects were more related to a limitation in ductility with increasing section size, as opposed to a reduction in hardness and strength. The effects of section size, as studied in this investigation, were not nearly as pronounced as the effects of alloy content and microstructure.

2. All trends in composition, microstructure and mechanical properties were analyzed separately for the 1 in. section size and for the 3 in. section size. Correlation Analysis as well as routines in the DOE analysis (Main Effect Plots, Pareto Charts, and Rejection Probability testing) showed that increasing Cu and/or Mn increased strength and hardness while decreasing ductility and toughness ($U_T$). In contrast, increasing Si decreased strength and increased ductility. However, varying Mn or Si was less effective than Cu in affecting the properties in the 1 in. section size.
3. The Pearson Correlation Analysis and various statistical routines conducted in the DOE showed that excellent variables and variable levels were selected for the DOE. Major effects and their magnitudes were clearly identified, or they were absent, so that strong conclusions could be drawn.
4. Based on the results of this study, the Principal Investigators chose to validate the DOE by casting 1 in. Y-blocks of Heat 6 (with 2.6%Si, 0.3%Mn and 0.6%Cu) at a different foundry. The results of the new repeat heat essentially duplicated the microstructure and tensile properties of the DOE Heat 6.
5. The Principal Investigators have also concluded that the results of this investigation mark the beginning of work that will ultimately result in a mathematical relationship (alloy factors) capable of predicting composition, structure, and mechanical properties. This conclusion is based on the fact that the DOE indicated that the variables selected, namely section size, silicon content, copper content and manganese content accounted for the main effects that were evaluated. Of course, substantially more variations than the "two levels" required for the DOE would be necessary to develop these relationships.
6. Heat treatment trials were conducted by intercritically austenitizing and subjecting the samples to

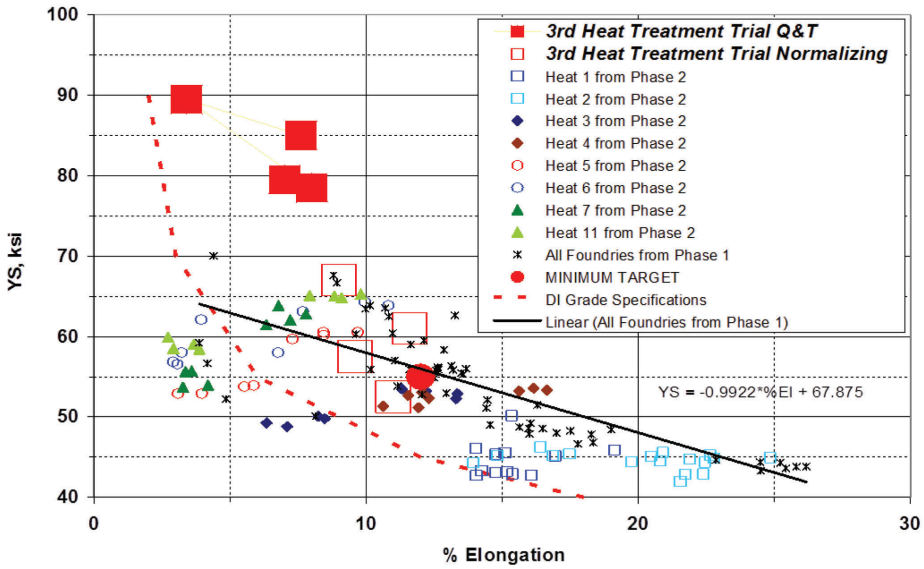


***Figure 42. Results of the Third Heat Treatment Trials with the as-cast data from Phase 2. Note that the heat treated samples (red) have greater strength and greater ductility than the as-cast commercial foundries line and the as-cast R&D castings.***

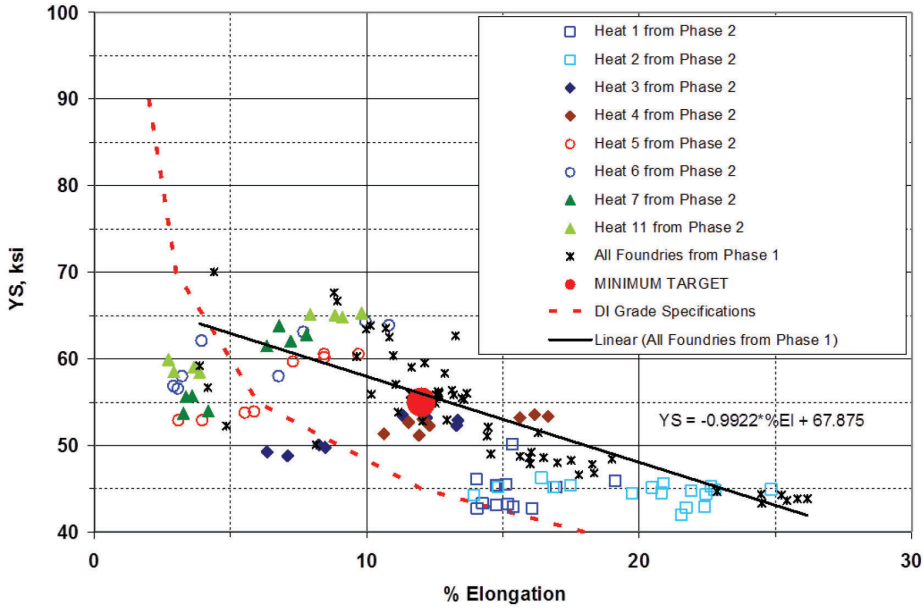


***Figure 43. Results of the as-cast data from Phase 2 versus commercial products from all the foundries of Phase 1 and the DI grade definitions. Note that the desired properties were obtained in several of the DOE heats.***

various cooling rates such as still air cool, forced air cool, and oil quenching, with the latter followed by tempering. The most promising results were obtained with a starting microstructure of 50% ferrite and 50% pearlite. After heat treatment, the measured mechanical properties far exceeded some of the study goals of >55 ksi YS, >80 ksi UTS and >12 % elongation. Even though 12% minimum elongation was not achieved through heat treatment, the quench and temper heat treatments produced much higher strength and equivalent ductility than many of the standard specifications for as-cast grades with lower strength. Mechanical properties obtained after intercritical austenitizing followed by either air cooling or quench and temper heat treatment were as follows: 65 to 85 ksi YS, 110 to 130 ksi UTS, and 8 to 9% elongation.

## Acknowledgements

The Principal Investigators gratefully acknowledge the funding, castings and other support that has been received from the American Foundry Society, The Ductile Iron Society, and the industrial sponsors: Betz Industries; Cadillac Casting, Inc.; Cast-Fab Technologies, Inc.; Caterpillar (CMO Plant); Elkem Metals, Inc.; Ellwood Engineered Casting Company; General Electric Energy; Hitachi Metals Automotive Components, USA LLC; Hodge Foundry, Inc.; Manitowoc Grey Iron Foundry; Neenah Foundry Co.; Parker Hannifin Corporation; Precision Metalsmiths, Inc.; Rio Tinto Iron & Titanium; Robar Industries, Inc.; Thyssen-Krupp Waupaca, Inc.; and Waukesha Manufacturing, Inc.

## REFERENCES

1. Goodrich, G.M., Lobenhofer, R.W., "Effect of Cooling Rate on Pearlitic Ductile Iron Mechanical Properties," *AFS Transactions*, vol. 115, pp. 547-566 (2007).
2. Goodrich, G.M., Lobenhofer, R.W., "Effect of Cooling Rate on Ductile Iron Mechanical Properties," *AFS Transactions*, vol. 110, pp. 1003-1032 (2002).
3. Tuttle, R.B. "Effect of Cooling Rate on the Mechanical Properties of a Fully Pearlitic Ductile Iron," *AFS Transactions*, vol. 118, pp. 243-264 (2010).
4. Gundlach, R. B., "Nodularity, its Measurement, and its Correlation with the Mechanical Properties of Ductile Iron, *Ductile Iron Society Research Report*, No. 37 (2006).
5. Goodrich, G.M., Tartaglia, J.M., Gundlach, R.B., "Phase 1 Report: Ductile Iron Structure-Property Relationships," Report Number CRS002079P (September 30, 2010).
6. Tartaglia, J.M., Gundlach, R.B., Goodrich, G.M., "Phase 2 Report: Ductile Iron Structure-Property Relationships," Report Number CRS002079P (December 23, 2011).
7. Tartaglia, J.M., Gundlach, R.B., Goodrich, G.M., "Optimizing Structure-Property Relationships in Ductile Iron," Report for Research Project No. 46, Ductile Iron Society, Strongsville, OH (August 2012).
8. Private Research conducted at Element, Wixom Michigan.
9. Gundlach, R.B., "Observations on Structure Control to Improve the Properties of Cast Irons," American Foundry Society Cast Iron Division Honorary Lecture (2008).
10. Dieter, G.E. "Mechanical Metallurgy," 3rd ed., McGraw Hill (1986).
11. Hall, E.O., Proceedings of the Physics Society, London, vol. 643 (1951).
12. Petch, N.J., "The Cleavage Strength of Polycrystals," *J. Iron Steel Institute*, London, vol. 173, pp. 25-28 (1953).
13. Armstrong, R.W., Chou, Y.T., Fisher, R.M., Louat, N., "The Limiting Grain Size Dependence of the Strength of a Polycrystalline Aggregate," *Philos. Mag*., vol. 14, issue 131, p. 943 (1966).
14. Nishi, S., Kobayashi, T., Taga, S., "The Effect of Microstructure on the Toughness of Ferritic Nodular Iron," *Journal of Materials Science*, pp. 723-730 (1976).
15. Zhou, J., Xie, Z., Zhong, F., "Effect of Austenitic Dendrites on Mechanical Properties of Ductile Iron," *Acta Metallurgica Sinica (English Edition)*, vol. 5, pp. 375-377 (1992).
16. Javaid, A., Davis, K.G., Sahoo, M., "Effect Of Chemistry And Processing Variables On Mechanical Properties Of Thin-Wall DI Castings," *AFS Transactions*, vol. 108, pp. 191-200 (2000).
17. Guo, X., Stefanescu, D.M., Chuzhoy, L., Pershing, M.A., Biltgen, G.L., "A Mechanical Properties Model for Ductile Iron," *AFS Transactions,* vol. 107, pp. 47-54 (1997).
18. Rezvani, M., Harding, R. A., Campbell, J., "Potential of Precipitation Hardening for Improving Mechanical Properties of Ductile Iron," *AFS Transactions*, vol. 105, pp. 183-189 (1997).
19. Cairioni, G., Silva, G., Tosi, G., Goria, C.A.,"The Influence of Certain Pearlitizing Elements on the Mechanical Properties of Ductile Iron," *Metallurgical Science and Technology*, vol. 1, issue 2, pp. 64-73 (1983).
20. Afrin, N., Chen, D. L., Cao, X., Jahazi, M., "Strain Hardening Behavior of a Friction Stir Welded Magnesium Alloy," *Scripta Mater*., vol. 57, issue 11, pp. 1004-1007 (2007).
21. AFS Cast Iron Division Committee 5I Report on the Effects of Different Alloying Elements, AFS Casting Congress (2010).
22. Grensamer, M., Pearsall, E.B., Pellini, W.S., Low, J.R., *Trans. ASM*, vol. 30, p. 1003 (1942).
23. Goodrich, G.M., Lobenhofer, R.W., "Effect of Cooling Rate on Pearlitic Ductile Iron Mechanical Properties," *AFS Transactions*, vol. 115, pp. 547-566 (2007).
24. Goodrich, G.M., Lobenhofer, R.W., "Effect of Cooling Rate on Ductile Iron Mechanical Properties," *AFS Transactions*, vol. 110, pp. 1003-1032 (2002).

25. Tuttle, R.B., "Effect of Cooling Rate on the Mechanical Properties of a Fully Pearlitic Ductile Iron," *AFS Transactions*, vol. 118, pp. 243-264 (2010).
26. Lenth, R.V., "Quick and Easy Analysis of Unreplicated Factorials," *Technometrics*, vol. 31, pp. 469-473 (1989).
27. Hayrynen, K.L., Keough, J.R., Kovacs, B.V., "The Effects of Alloying Elements on the Critical Temperatures in Ductile Iron," Ductile Iron Society, Research Report No. 22 (December 1997).
28. Shewmon, P.G., Transformations in Metals, McGraw-Hill, New York, NY, pp. 226-228 (1969).
29. Howell, P.R., "The Pearlite Reaction in Steels: Mechanisms and Crystallography," *Materials Characterization*, vol. 40, pp. 227-260 (1998).
30. Zanardi, F., "The Development of ADI and IDI in Italy," AFS/DIS 2008 Keith Millis Symposium on Ductile Cast Iron (2008).